The galactic rotation curve derived from observations of neutral hydrogen

Shane, W.W.; Bieger-Smith, G.P.

1966, *Bull. Astr. Inst. Netherlands* **18** 263–292;
Communication from the Netherlands Foundation for Radio Astronomy and the Observatory at Leiden

THE GALACTIC ROTATION CURVE DERIVED FROM OBSERVATIONS OF NEUTRAL HYDROGEN

W. W. SHANE and G. P. BIEGER-SMITH

Received 15 October 1965

Fifty profiles of the twenty-one centimetre line of neutral hydrogen have been obtained between longitudes $l^{II} = 22°.3$ and $70°.0$ in the galactic plane using the twenty-five metre radio telescope at Dwingeloo. From these profiles a contour map of brightness temperature as a function of longitude and velocity has been prepared. The cut-offs of the line profiles at positive velocity have been studied with the aim of obtaining a galactic rotation curve applicable on the east side of the centre. Two sorts of models have been discussed in detail. The first, represented by model V in the following text, ascribes the irregularities in the observed curve to hydrogen density variations alone and leads to an improbably sharp contrast between the hydrogen density in the spiral arms and in the inter-arm region. The second sort of model, number VII and its modifications, attributes the irregularities to large-scale motions which may be associated with the spiral structure, such as a systematic difference in motion between the gas located in and between the spiral arms. In the region in which the Sagittarius arm is seen tangentially, this motion may take the form of a stream of gas moving along the outer edge of the arm in the direction of galactic rotation with a velocity between 5 and 10 km/sec greater than that of the arm itself; BURTON (1966) has suggested such a possibility on the basis of a detailed survey of the region. In this case, the velocities given by the model VII rotation curve will be somewhat higher than the velocities in the arms themselves. This interpretation does not place such severe restrictions upon the hydrogen density distribution and leads in a more plausible picture. All models lead to maximum velocities at least as high as those previously determined for the region east of the centre and thus confirm the apparent large-scale differences between the eastern and western quadrants. The principal results of the computations are shown in table 5 and figure 12.

1. Introduction

The first determination of the galactic rotation curve from 21-cm observations was made by KWEE, MULLER and WESTERHOUT (1954). It was confined essentially to the part of the Galaxy east of the galactic centre ($l^{II} > 0°$) and inside the solar circle. Subsequently KERR (1962) analysed the Sydney observations (KERR, HINDMAN and GUM, 1959) of the region west of the centre ($l^{II} < 0°$) and derived a somewhat different rotation curve than that found from the Leiden observations. He pointed out that it was possible to account for this difference and retain large-scale symmetry in the pattern of hydrogen distribution only by assuming that the "local centre of rest" as defined by the average motion of stars and gas in the neighbourhood of the Sun is moving outward from the galactic centre with a velocity of 7 km/sec. This interpretation has been criticized as incompatible with optical determinations of the local solar motion (e.g. FEAST, 1964). KERR (1962) has suggested an observational test of the hypothesis that such an expansion is a general feature of galactic kinematics, and BRAES (1963) has carried out a related test. The results were not consistent with the hypothesis of general expansion, but the possibility of a local outward movement could not be eliminated. AGEKYAN *et al.* (1964) have applied a new method of analysis to the Leiden and Sydney observations at all latitudes and have derived a revised rotation curve in the region $5.7 \text{ kpc} < R < 12.5 \text{ kpc}$.

Recent observations by KERR (1964, 1965) have confirmed the apparent asymmetry with respect to the galactic centre. Over the whole region from 30° to 53° from the centre the two rotation curves show strikingly similar behaviour, with a separation in good agreement with the value predicted by the expansion model. Outside this region, however, the curves no longer conform to the predicted pattern. Less than 30° from the centre, where the difference is expected to be greatest, the two curves nearly coincide, while beyond 53° from the centre the difference has the opposite sense. These observations require us to accept a picture of the Galaxy in which large-scale asymmetries are present. In view of this conclusion and the optical evidence, we have decided to make the usual assumption that

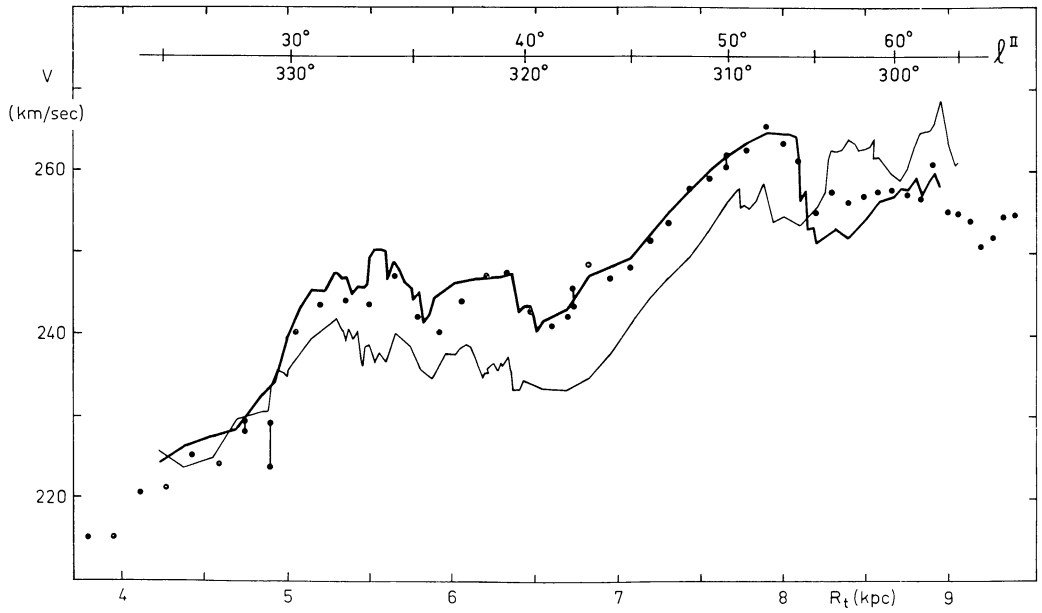

Figure 1. The galactic rotation curve derived by KERR (1964, 1965). The velocities correspond to points half way up the steep edge of the galactic equator profiles. The heavy and light curves correspond to observations on the east and west sides of the galactic centre respectively. The filled circles were derived from the observations discussed here. Double values correspond to alternative adopted values for the heights of the final peaks.

the motion of the local standard of rest is 250 km/sec in the direction $l^{II} = 90°$. The effect of any other assumption is easily calculable.

Dr. Kerr has sent us his newly derived rotation curve (KERR, 1965) based on the revised distance scale, and we have reproduced it, with his kind permission, as figure 1. The heavy curve represents Kerr's observations on the east side of the centre. The new observations discussed in this paper have been treated as nearly as possible in the same way as those of Kerr and are plotted as filled circles. The ordinate is the velocity with respect to the galactic standard of rest [cf. equation (24)] of the point on the steep edge of the profile where the brightness temperature reaches half its maximum value. The abscissa is the galactic longitude* l of the observation and the corresponding galactocentric distance R_t of the tangent point. The Leiden observations plotted as double points correspond to cases of uncertainty regarding the selection of the maximum brightness temperature. The lower point corresponds to selection of the highest maximum and the upper to selection of a prominent secondary peak. In view of the difference in resolution between the two sets of observations, we consider the agreement to be very satisfactory.

The available optical data bearing on the problem of the rotation curve have recently been subjected to careful analysis by FEAST and SHUTTLEWORTH (1965). They have been able to explain the greatest part of the difference between the optical and 21-cm rotation curves as noted, among others, by MÜNCH and MÜNCH (1960), as the systematic effect of random errors in the optical distance determinations. Combining optical data from both sides of the galactic centre, they derive a rotation curve which does not differ significantly from the Sydney curve (KERR, 1962). The Leiden curve (KWEE, MULLER and WESTERHOUT, 1954) remains about 5 km/sec higher. We are grateful to the authors for letting us see these valuable results in advance of publication.

The Leiden rotation curve derived by KWEE, MULLER and WESTERHOUT (1954), hereafter referred to as KMW, was derived from line profiles in the galactic plane at 35 longitudes between $l = 353°.4$ and $77°.3$. The following procedure was used.

* Galactic coordinates will ordinarily be expressed in the revised system (l^{II}, b^{II}) which will henceforth be written without superscripts.

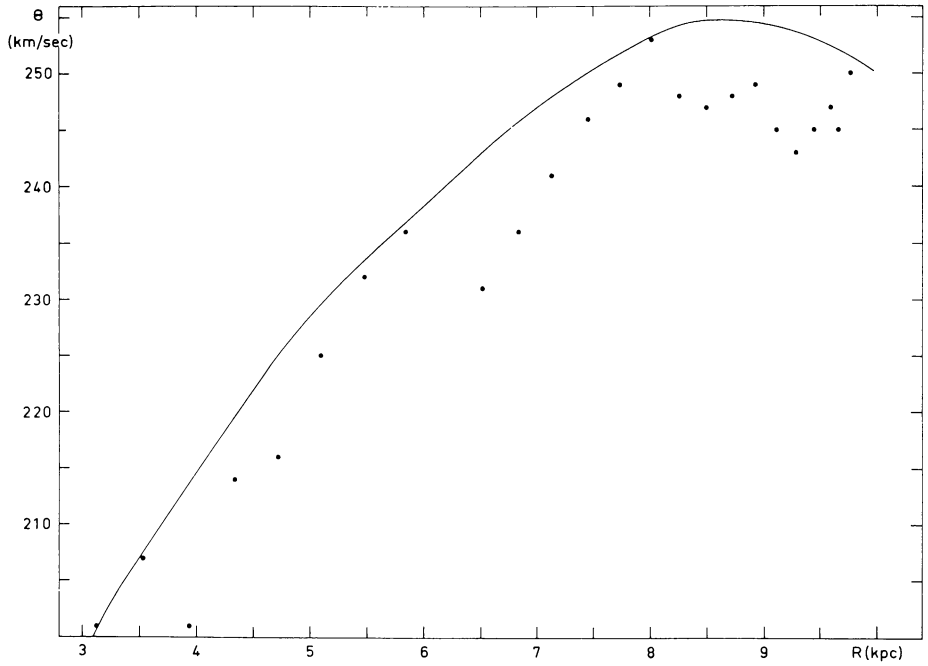

Figure 2. The galactic rotation curve derived by KWEE, MULLER and WESTERHOUT (1954). The drawn curve is the adopted KMW rotation curve, and the points show the values of $\Theta_c(2)$ calculated from equation (3) and indicate the deviations from the expected maximum velocities. This figure differs from that originally published by Kwee, Muller and Westerhout only in so far as it is based upon the revised galactic parameters, $R_0 = 10$ kpc and $\Theta_0 = 250$ km/sec.

1) Assuming a gas temperature $T_g = 125$ °K, the observed brightness temperatures T_b were converted to optical depths τ by means of the relation

$$\tau = -\ln\left(1 - \frac{T_b}{T_g}\right). \qquad (1)$$

The velocity scale was corrected for the standard solar motion.

2) Representing the velocity about the galactic centre Θ by an approximation depending only upon the distance R from the centre $\Theta_a(R)$ and assuming a uniform hydrogen distribution, model line profiles of optical depth as a function of velocity were calculated.

3) These profiles were smoothed by a Gaussian distribution function. The Gaussian form and the dispersion were chosen to give the best match to the observed profiles.

4) The observed and calculated profiles were normalized to the same maximum height, and the velocity shift ΔV was determined which, when applied to each calculated line profile, brought it into the best coincidence with the observed profile.

5) The observed maximum velocity at each longitude l was taken to be

$$V_{max} = \Theta_a(R_0 \sin l) + \Delta V(l) - \Theta_0 \sin l, \qquad (2)$$

where R_0 is the distance from the Sun to the galactic centre and Θ_0 the velocity of the local standard of rest about the centre.

If the hydrogen distribution along the lines of sight in the neighbourhoods of the tangent points, which are the points at which the lines of sight pass closest to the centre, is approximately uniform and not very much less than the hydrogen density elsewhere, and if the hydrogen moves in circular orbits about the galactic centre such that the angular velocity never increases outward, then the maximum velocities observed will be those corresponding to the tangent points. These conditions are fulfilled by the model. If they are fulfilled in reality we may derive the rotational velocity Θ_c at each distance from the centre corresponding to an observed tangent point

$$\Theta_c(2) = V_{max}(l) + \Theta_0 \sin l = \Theta_a(R_0 \sin l) + \Delta V(l). \qquad (3)$$

These velocities are plotted as points in figure 2, which is derived from figure 7 of KMW with scale changes to adapt it to the revised system of galactic parameters (I.A.U. 1964), $R_0 = 10$ kpc and $\Theta_0 = 250$ km/sec. The distribution of the points in this diagram suggested the model proposed by KMW: that we see hydrogen concentrated in two spiral arms which are visible tangentially at $l = 38°$ and 53° respectively, in a central disk and in the neighbourhood of the Sun. This model is shown schematically in figure 8 of KMW. Such a model would permit a smooth rotation curve $\Theta_c(R)$ to be drawn, passing through the highest observed points in figure 2, where hydrogen is found near the tangent points and remaining above the intervening observed points, which are depressed through the absence of hydrogen from the tangent region. The distances by which these points are depressed below the smooth curve will measure the tilt of the inner boundaries of the arms. Using the data from KMW we have made this calculation and find for the inner arm a tilt of 61° (67° if the two innermost points are neglected) and for the outer arm 78° (74° if the outermost point is neglected). These values are much smaller than those normally found for the tilt of the arms from 21-cm studies (see, for example, SCHMIDT, 1957, who finds from closely related material a tilt of about 84° for the outer, so-called Sagittarius arm) and result in the arms falling surprisingly close together. The large tilt of the inner arm must be attributed to a local disturbance, for if we extrapolate this arm a short distance outward, we see that, even assuming that it is very narrow, it will still be easily visible just on the near side of the tangent point at $l = 41°$, a direction in which the observations show a velocity discrepancy of 13 km/sec.

Admitting the possibility of an irregular hydrogen density distribution, the model proposed by KMW appears to represent the observations in a plausible way. Thus a rotation curve drawn through the highest observed points was adopted as final. This curve, adjusted to the revised galactic parameters, is plotted in figure 2 and tabulated for $3.8 \leqslant R \leqslant 10.0$ kpc in column 2 of table 5. It has been suggested (e.g. KERR, 1962) that the difference between the Leiden and Sydney rotation curves may be due, at least in part, to the procedure described above, but, as we have seen, the new observations of KERR (1964, 1965) indicate that, whatever the cause of the apparent asymmetry, the difference in measured rotational velocity is real.

2. Observations and reductions

The discovery of the expanding or 3-kpc arm by VAN WOERDEN *et al.* (1957) led to the initiation in 1958 of a programme to survey in detail the distribution of neutral hydrogen in the region between 4 and 7 kpc from the galactic centre (SHANE, 1966). An essential part of that programme was a redetermination of the rotation curve using the improved resolution available with the 25-metre radio telescope at Dwingeloo. In view of the uncertainties that have arisen concerning the interpretation of the original Leiden rotation curve, it seems appropriate to discuss these observations separately. The first observations, line profiles at 21 longitudes in the galactic plane between $l = 22°.3$ and 42°.3, were made in early 1959. At the suggestion of Dr. G. Westerhout a second group of 29 longitudes between $l = 42°.0$ and 70°.0 was observed during 1961. All observations were made using the 8-channel 21-cm line receiver on the Dwingeloo 25-metre telescope. The telescope and receiver and the observing and reduction procedures have been described most recently by RAIMOND (1966) and need not be fully discussed here. The half-power beamwidth of the antenna at 21 cm is 0°.56 and the setting accuracy about 0°.03. The first series of observations was made along the latitude circle $b^{\mathrm{I}} = -1°.5$, resulting in a deviation from the new galactic plane of up to 0°.13 in the neighbourhood of $l = 40°$. This deviation will have no significant effect on the determination of galactic rotation, but the line profiles will differ in some detail from profiles at $b^{\mathrm{II}} = 0°.0$. All observations were made with an equivalent bandwidth of 10 kc/s and all points except those at the extreme ends of the profiles were observed separately on at least two channels by letting the intermediate-frequency oscillator sweep over at least twice the 50 kc/s channel separation. All observations are complete from zero velocity to well beyond the positive limit of the hydrogen velocities. The observations are represented by brightness temperatures measured at intervals of 5 kc/s. Following RAIMOND (1966) and assuming that each point is measured twice, we can estimate the r m.s. noise of a single point as $\mu(T_b) = \pm 0.5$ °K. Further, all corrections described by Raimond have been applied here except as noted below.

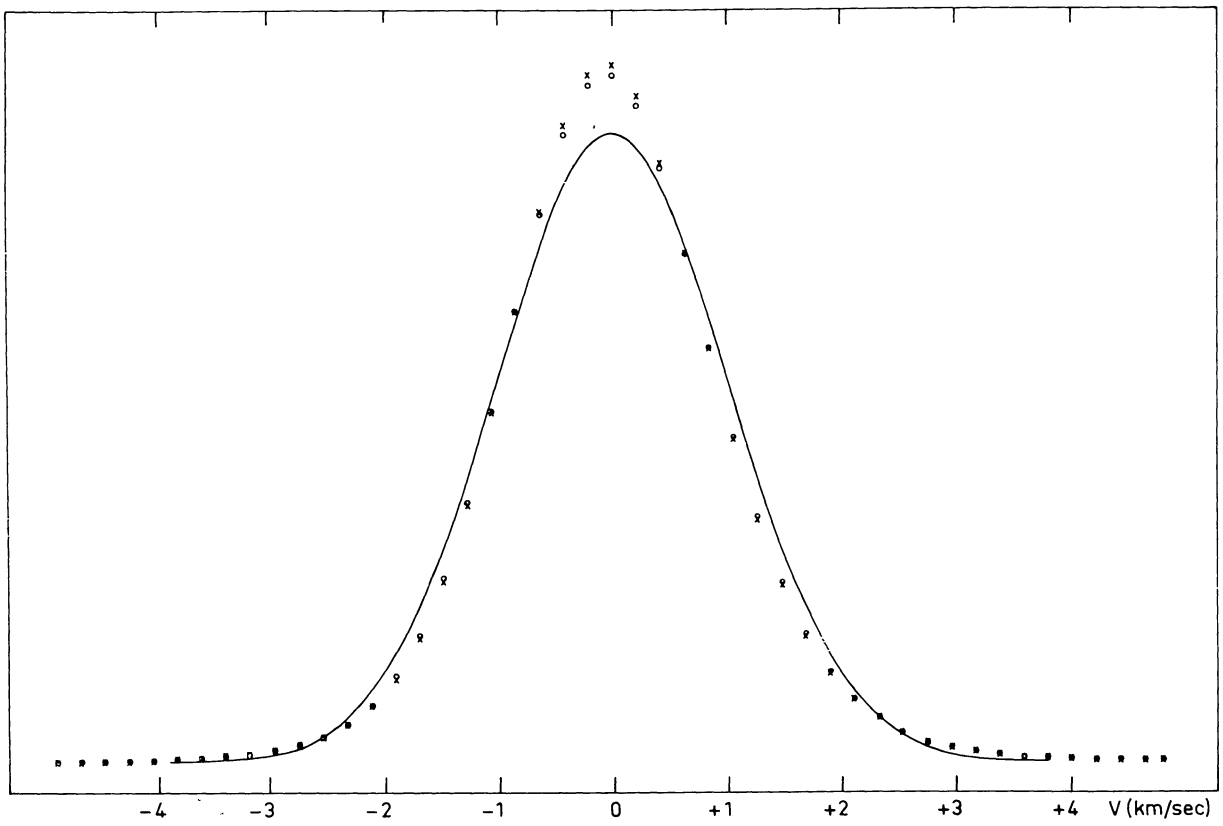

Figure 3. The velocity smoothing profile. The crosses and open circles define the effective smoothing profiles as applicable to the observations discussed here. The solid curve, a Gaussian profile with a half-width of 2.36 km/sec, is shown for comparison.

No account has been taken of possible effects of line radiation in the side-lobes as discussed by VAN WOERDEN *et al.* (1962), the effect of which was not recognized until after the observations described here had been reduced. The maximum expected correction of about 1 °K will have no appreciable influence on the results presented here. The effect is likely to have its greatest influence in the neighbourhood of $l = 60°$, where the galactic anticentre will lie in the spillover lobe.

No attempt has been made to correct the observations for smoothing effects either in position or velocity. The spacing between observations is too great to permit unsmoothing in longitude where the run of intensities is not predictable. Systematic corrections could have been applied to account for the fact that the intensity will drop off appreciably on either side of the galactic plane within the antenna beam, but this was not done as it was not the purpose of this study to determine the mean hydrogen density in the plane. Supposing that the hydrogen is distributed smoothly and symmetrically with respect to the plane with a half-width of 280 pc (SCHMIDT, 1957), the correction at maximum velocity will vary smoothly from 10 per cent at $l = 22°.0$ to 0.7 per cent at $l = 70°.0$.

Instrumental smoothing in velocity has been introduced in three ways. The primary source of smoothing is the receiver passband, whose shape as a function of displacement Δv in kc/s from its centre is given to a good approximation by the empirical formula $[(\Delta v)^2 + (6.8)^2]^{-3}$. The effective bandwidth is about 10 kc/s. Secondary sources of smoothing are the time constant filter in the final stage of the receiver and the averaging of the recorded intensities over intervals of about one half bandwidth.

The net smoothing profiles for the two methods of averaging used in this programme are shown in figure 3 as crosses and open circles. They are characterized by $\langle(\Delta v)^2\rangle = 22.51$ and 22.95 $(\text{kc/s})^2$ respectively. The

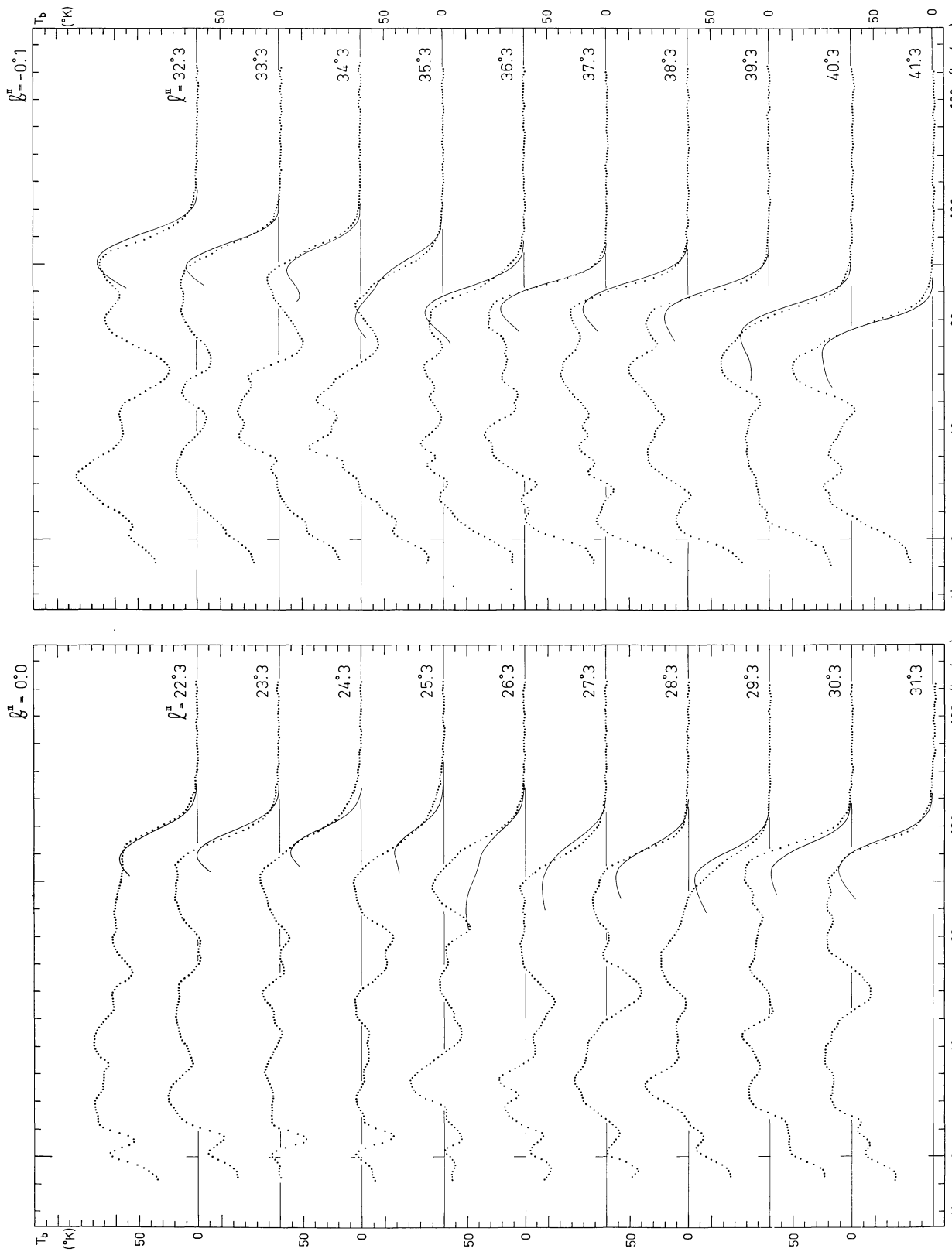

Figure 4. The observed line profiles. The observed brightness temperatures are plotted as points as a function of velocity with respect to the local standard of rest. The latitudes and longitudes of the observations are shown. The solid curves are line profiles predicted on the basis of model VII.

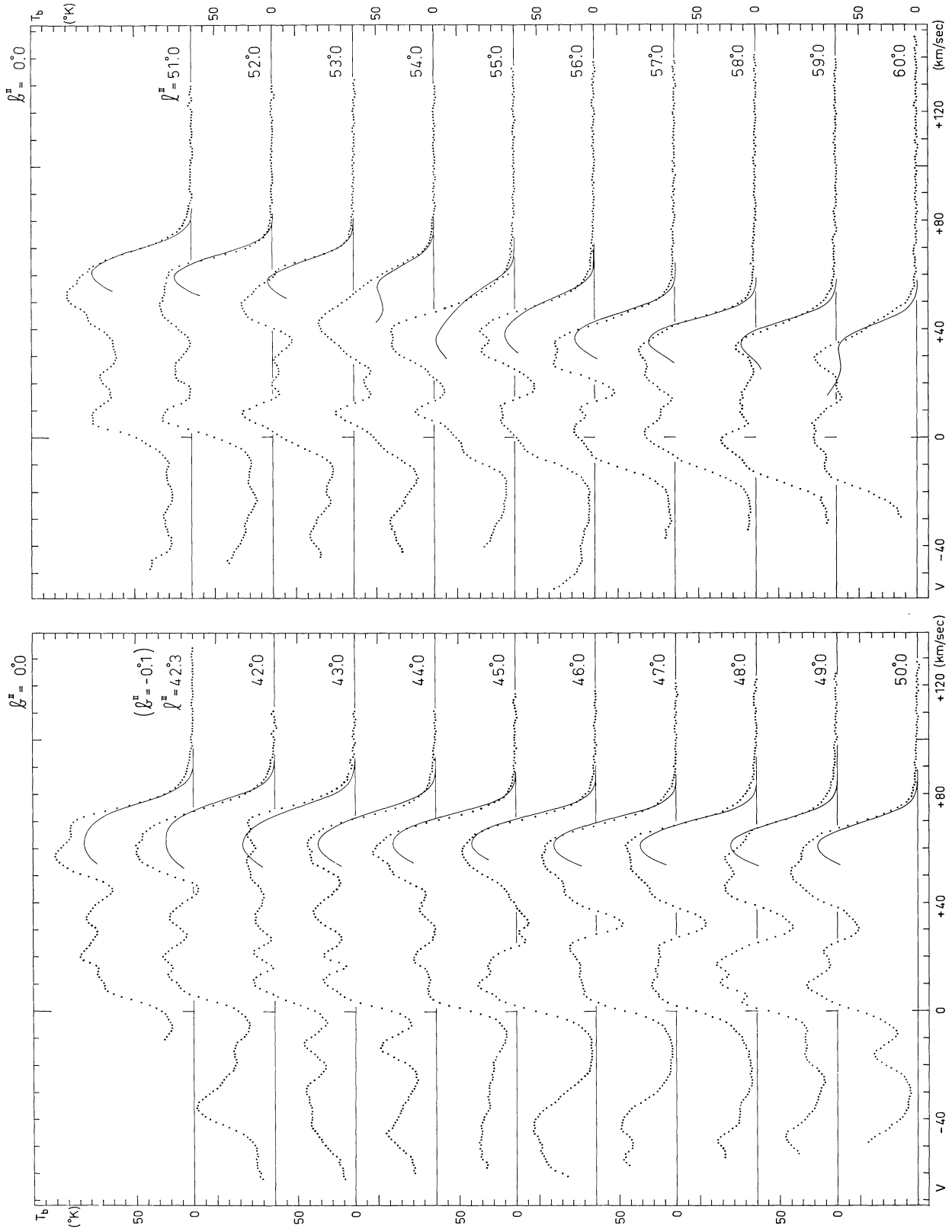

Figure 5. The observed line profiles (*continued*).

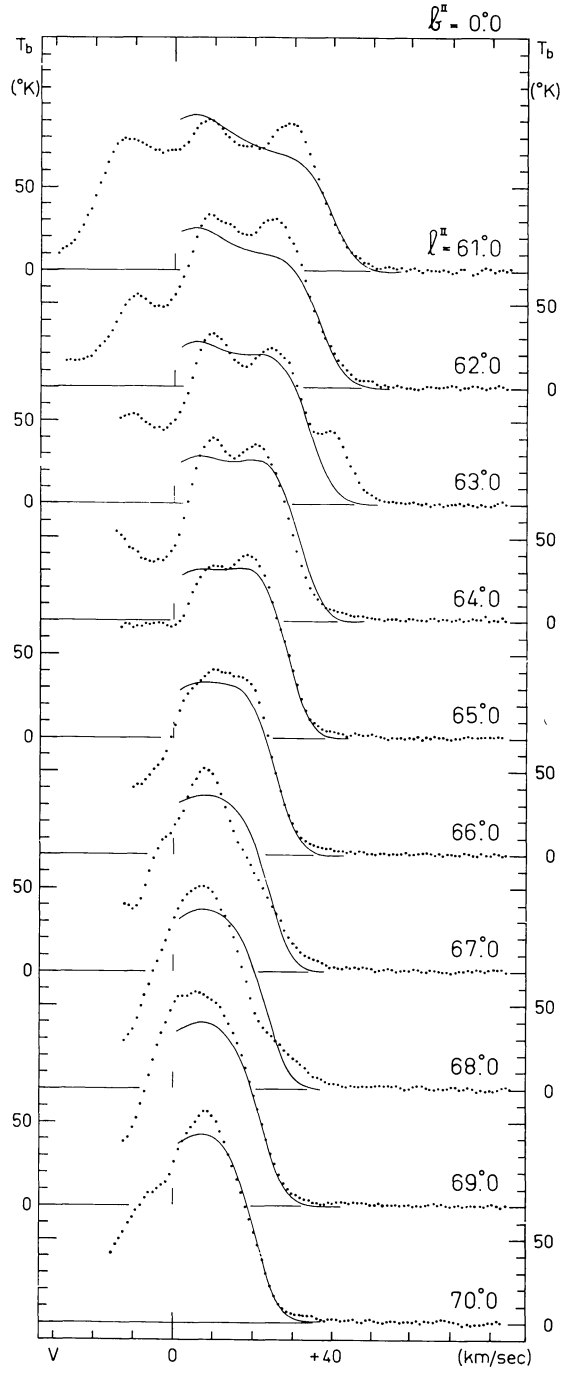

Figure 6. The observed line profiles (*continued*).

solid curve is Gaussian with the square of the dispersion $\sigma^2 = 22.73$ (kc/s)^2 and thus a width between half-power points of 2.36 km/sec, which is a measure of the effective velocity smoothing. This instrumental smoothing will tend to increase slightly the observed smoothness of the line profiles, but if the intrinsic smoothing profile has a half-width of the order of 15 km/sec, as we have assumed, the instrumental effects will increase this by only about 2 per cent.

The observed line profiles are reproduced in figures 4–6 in the form used in the Dwingeloo atlas of line profiles, part I of which, including explanatory material, has been published by VAN WOERDEN *et al.* (1962). They will be reprinted in a forthcoming part of the atlas. The ordinate is expressed in the units defined by HÖGBOM and VOLDERS (1961), where 1 unit $\approx$ 1 °K (brightness temperature). Keeping in mind the reservations voiced by Högbom and Volders, we will assume that 1 unit = 1 °K and express brightness temperature in °K. The abscissa is expressed in km/sec with reference to the local standard of rest, assuming the standard solar motion. The positions are given in the new system of galactic coordinates, and the tendency for the first series of observations to fall at slightly negative latitudes is apparent. In addition to the observations, which are shown as points at intervals of 5 kc/s, we have also plotted expected line profiles as computed from a galactic model. These profiles will be discussed in section 4.4.

The observed values of T_b are expected to be 0 °K for the high-velocity extremes of the line profiles, but some profiles show substantial deviations from zero at high velocities. This is particularly true of the profiles at $l = 31°.3$, $33°.3$ and $40°.3$, all of which seem to be more than 1° too low. This is probably due to uncertainties in determining the instrumental zero line during the first observing period (1959). Between 1959 and 1961 instrumental improvements had made possible more accurate control of the zero level. No empirical corrections have been applied to the measurements with apparent zero line errors, as the frequency dependence of the required correction is unknown, but account of the effect has been taken in some of the following calculations. In addition to the three profiles listed above, several others of both series show zero line deviations of 1 °K or less. No further account has been taken of these effects. The profiles at $l = 42°.3$, $61°.0$ and $62°.0$ extend to higher velocities than shown. The high-velocity portions of the profiles show no significant deviations from zero temperature and have been omitted from the figures. Otherwise the observations are shown in their entirety.

All the observational data have been combined in a single contour map, figure 7. The ordinate is velocity relative to the local standard of rest, and the abscissa is longitude. The latitudes at which the observations were made are indicated along the lower edge of the map. The small figure in the upper left corner shows the half-power resolution of the telescope and receiver. It should be noted that the actual resolution in longitude is limited by the 1° spacing between measurements. The contour interval is 2 °K in brightness temperature for $T_b \leqslant 10$ °K and 5 °K for higher values. Heavy contour lines correspond to intervals of 20 °K. Broken contours enclose regions of low brightness temperature.

The major features of galactic structure found from other 21-cm studies (e.g. WESTERHOUT, 1957) can be identified on this map, although the great amount of detail shown here makes the picture exceedingly complicated. In this paper we will be concerned only with the upper boundary of the body of radiation shown, specifically the drop-off toward higher velocities from the high-velocity maximum. The most prominent features of this part of the diagram are the general wavy appearance of the contours, which will be considered in the following discussion, and the remarkable projection to higher velocities at $l = 63°$. This latter is apparently a very strong isolated high-velocity feature. A further study of this feature has been initiated and the first observations show that it extends with decreasing brightness two or three degrees on either side of the galactic plane and fans out to about an equal extent in longitude. In the present study we have tried to eliminate the influence of this exceptional feature in so far as possible, as being atypical of the general hydrogen motion, but we must keep in mind the possibility that this may well be only the most prominent example of a more frequently occurring phenomenon. Less prominent features of the same sort will not be so easily separable from the general structure but will strongly influence the form of the line profiles.

3. Analysis of the line profiles

In order to interpret the observations in terms of galactic hydrogen distribution and kinematics, we have compared the observed line profiles with profiles computed from galactic models based upon various sets of assumptions. These models will be discussed below; the line profiles derived from one of them are plotted as solid curves in figures 4–6.

The comparisons have generally been made in two ways, as follows.

1) The observed and computed line profiles are compared directly over the region of interest. Corrections to proposed models can often be derived by noting the distance along the velocity axis by which a computed profile must be shifted and the factor by which the ordinate must be multiplied in order to bring it into the best agreement with the observation.

2) A quantitative measure, useful for comparing velocities, is the terminal velocity V_x defined by the expression

$$V_x = V_M + \frac{1}{Y_M}\int_{V_M}^{V_+} Y(V)\,dV, \qquad (4)$$

where V_M is the velocity of the highest velocity maximum of the profile, Y_M is the corresponding ordinate, V_+ is a velocity high enough that the ordinate has fallen to zero (usually taken as the end of the observed profile) and $Y(V)$ is the ordinate at any velocity V. For computation the integral is replaced by a sum

$$V_x = V_M - \frac{\Delta V}{2} + \frac{1}{Y_M}\sum_{V_M}^{V_+} Y(V)\Delta V. \qquad (5)$$

This measure has the advantage over other velocity measures, such as the velocity at which the ordinate reaches half its maximum value, that here we use all the available data from the line profile to determine a characteristic velocity, not just the velocity at one or two selected points. It is essentially free from systematic effects due to noise (which can lead only to a slight overestimate of Y_M) and scale error. The effect of zero line error, on the other hand, can be significant.

Of these two methods, the second is the more objective and yields a numerical result directly, while the first, by its very subjectivity, permits us to make allowance for irregularities in the shapes of the observed profiles and weight most heavily those parts which appear to be least disturbed by extraneous features. Even in the determination of V_x a degree of arbitrariness is introduced by the choice of V_M. The great path length over which the observed radial velocity remains near its maximum value leads us to expect a pronounced

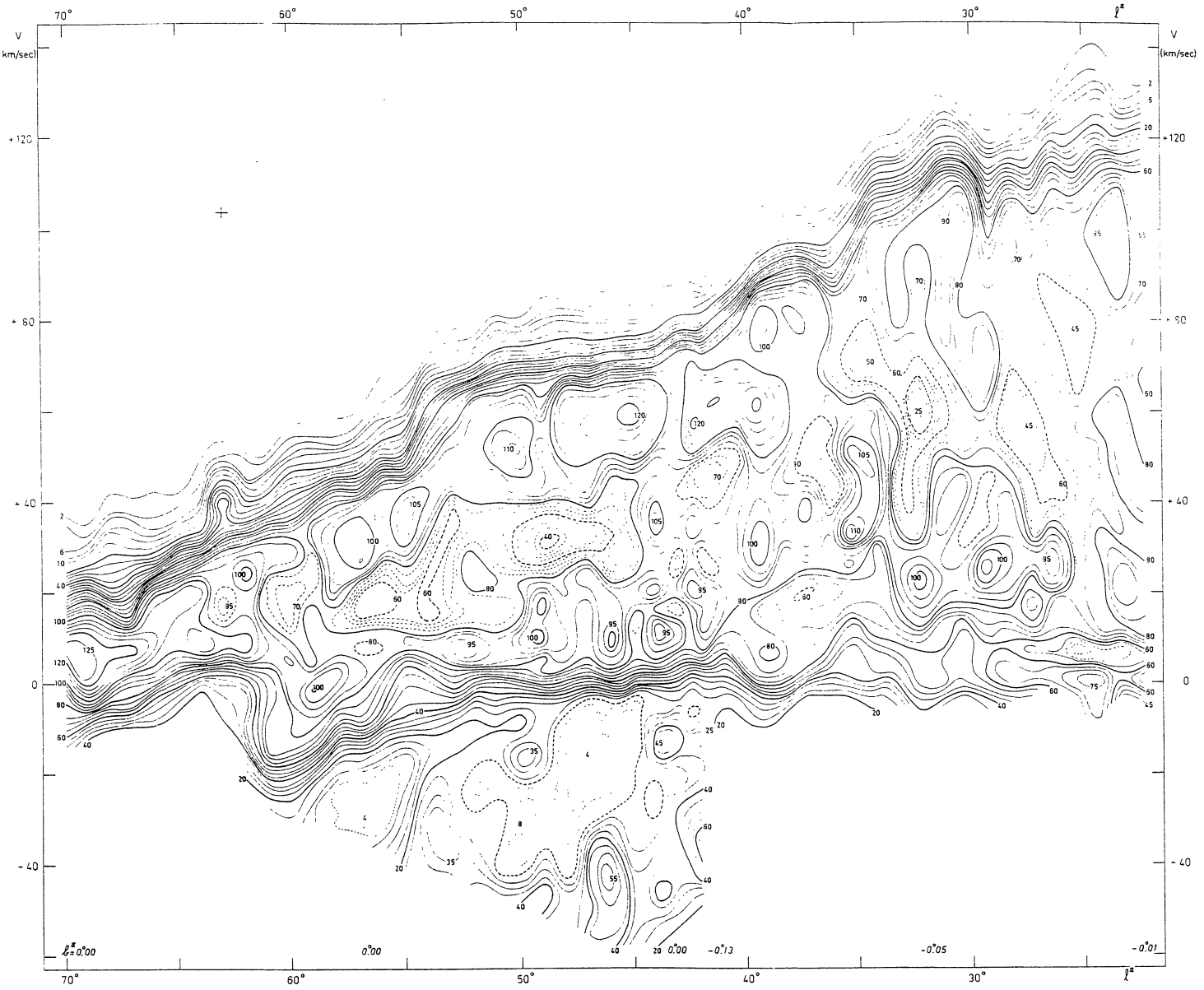

Figure 7. Contour map of brightness temperature in the galactic plane. Brightness temperature as a function of velocity and galactic longitude is shown in the form of a contour map. The contours for each 2 °K of brightness temperature below 10 °K and for each 5 °K for higher values are shown. The contours corresponding to each 20 °K are heavily drawn. Broken lines enclose regions of low brightness temperature. Small deviations from the galactic plane are indicated by values of b^{II} shown along the lower margin. The small figure in the upper left corner shows the instrumental resolution to half power. The true resolution in longitude is limited by the one-degree spacing of the observations.

maximum in each line profile near its high-velocity termination. Such a maximum is indeed present in almost all cases, but it is often of such an irregular form that it is not clear which point should be taken as V_M. Some of the effects which may distort the ideal picture are discussed below.

1) The hydrogen density in the neighbourhood of the tangent point may be sufficiently low in comparison with other regions that the peak is lowered or disappears. In general some flat or gently sloping shoulder will remain, and in this case the high-velocity edge of the shoulder should be taken as V_M. This effect may account for the profiles at $l = 22°.3$ and $29°.3$. The hydrogen density may, in fact, be so low in the tangent region that only a low-lying extension to the line profile is visible. No clear case of this has been observed, but something of the sort might explain the profiles at $l = 67°.0$ and $68°.0$. In more extreme cases we might observe no extension at all. Models with low hydrogen density over large regions will be discussed in section 4.3.

2) A concentration of hydrogen not far from the tangent point will introduce a peak into the line profile at a velocity somewhat lower than that of the peak in the case of uniform distribution. The peak corresponding to the tangent velocity may remain visible as a shoulder, in which case the velocity of this shoulder should be taken as V_M. If the hydrogen concentration is quite close to the tangent point, the shoulder may no longer be identifiable, but the error made by adopting the peak in this case will not be large. The profiles at $l = 41°.3$ and $42°.3$ show structure which might be attributed to this effect.

3) Small-scale streaming motions are indistinguishable from turbulent smoothing, but if the extent of such streams is comparable with the beamwidth or larger (about 50 pc at these distances) the effect will be to shift the whole profile or to introduce separate components with the corresponding velocities. Presumably the extension at $l = 63°.0$ is such a component. The form of the observed line profile will depend upon the distribution of streaming velocities. If the stream with the greatest projected velocity along the line of sight contains a major part of the hydrogen near the tangent point, then it is this component which will dominate. If the highest velocity stream contains only a small part of the hydrogen, it may still show up as a low shoulder or extension such as we observe at $l = 67°.0$ and $68°.0$. In intermediate cases, shoulders or extensions of various heights may be observed. The velocity measured from such a profile will depend upon the part of the profile that is considered. If equation (5) is used, then the choice of V_M will determine the extent to which we restrict our attention to the streams of highest velocity. Such a restriction will generally result in the measurement of a velocity higher than the average in the neighbourhood of the tangent point. In practice it is seldom possible to determine whether the irregularities observed in the line profiles are due to these effects or to those discussed under 2) above, where the prejudice will be toward assignment of too low a velocity.

We have kept these considerations in mind when comparing the results of our model calculations with the observations. When using direct comparison of line profiles, we have tried to achieve the best match for that part of the profile below any high shoulder. In many cases the peaks have then failed to match, but we have attributed this to hydrogen density variations outside the tangent region, which were not incorporated in the model. If, in fact, the irregular form of the line profile is due to gas streaming, then we have measured a velocity corresponding to the component of the gas with the highest velocity. Where even the higher velocity parts of the observed profiles were of such a form as not to be reproducible by the models, we have tried to make a reasonable compromise. The profiles at $l = 67°.0$ and $68°.0$ were particularly troublesome in this respect. Similarly, in choosing values of V_M, preference was given to prominent high shoulders over actual maxima. In many cases, two values of V_M were chosen and the corresponding values of V_x were computed. In most of the following discussion both values are used and it will be seen that the difference between them may be considerable, sometimes amounting to 5 or even 10 km/sec. Where it was necessary to determine a unique value of V_x, that corresponding to a high shoulder was chosen in preference to an actual peak or a low extension. In two cases the means of two values have been adopted.

The values of V_x were determined in two ways for each line profile, once with the ordinate expressed in optical depth, computed from the observed line profiles using equation (1) under the assumption that $T_g =$

TABLE 1
Observed and computed terminal velocities

(1) ℓ^{II}	(2) V_c (km/sec)	(3) V_x (km/sec) Observed τ-profiles	(4) Computed model I	(5) V_x (km/sec) Observed T_b-profiles	(6) Computed model VI	(7) Computed model VII
22°3	116.4	119.4 S	120.5	120.4 S	122.2	118.9
23.3	114.8	114.7 P	119.2	116.9 P	120.6	119.1
24.3	113.2	114.6 P	117.5	117.4 P	119.1	120.0
25.3	111.6	112.8 P	116.0	114.6 P	117.5	119.9
26.3	109.9	112.1 P	114.4	114.5 P	115.8	113.9
27.3	108.1	108.2 P	112.5	109.7 P	114.0	114.2
28.3	106.2	109.9 S	110.5	111.1 S	112.1	112.9
				(110.1) P		
29.3	104.3	105.1 S	108.6	106.9 S	110.2	111.8
		95.8 P				
30.3	102.3	112.9 P	106.5	114.1 P	108.2	114.1
31.3	100.3	115.0 S	104.7	116.9 S	106.2	116.1
		112.6 P		(114.5) P		
32.3	98.3	108.8 P	102.7	110.4 P	104.2	111.6
33.3	96.2	105.6 S	100.6	107.8 S	102.1	108.3
34.3	94.0	104.5 P	98.4	106.3 P	99.9	107.1
35.3	91.8	99.0 S	96.1	99.9 S	97.7	98.7
		96.6 P		(97.9) P		
36.3	89.5	90.9 P	93.7	92.3 P	95.4	92.8
37.3	87.2	91.1 P	91.5	92.4 P	93.1	93.4
38.3	85.0	90.3 P	89.2	92.0 P	90.9	94.1
39.3	82.9	87.8 P	87.2	89.7 P	88.8	91.5
40.3	80.7	82.9 S	85.1	84.9 S	86.6	85.6
		77.6 P		(82.8) P		
41.3	78.5	78.0 S	82.7	79.2 S	84.4	79.1
		73.2 P		(76.6) P		
42.3	76.3			77.7 S	82.2	76.8
42.0	77.0	72.5 S	81.3	76.2 S	82.9	77.7
		70.6 P		(75.6) P		
43.0	74.8	76.3 P	79.2	77.9 P	80.7	75.4
44.0	72.6	70.5 P	77.0	73.2 P	78.6	74.0
45.0	70.5	68.0 S	74.9	72.5 S	76.4	73.1
				(71.5) P		
46.0	68.3	68.2 P	72.8	72.6 S	74.2	72.4
				(71.7) P		
47.0	66.2	67.2 P	70.7	71.1 S	72.1	71.7

(1) ℓ^{II}	(2) V_c (km/sec)	(3) V_x (km/sec) Observed τ-profiles	(4) Computed model I	(5) V_x (km/sec) Observed T_b-profiles	(6) Computed model VI	(7) Computed model VII
48°0	64.0	68.3 P	68.4	72.2 S	69.9	71.0
				71.5 P		
49.0	61.8	71.4 S	66.2	73.1 S	67.7	70.7
		67.7 P		(70.6) P		
50.0	59.7	67.8 S	64.1	70.3 S	65.5	70.3
		64.8 P				
51.0	57.5	64.4 P	62.0	69.5 S	63.4	70.3
				(68.3) P		
52.0	55.3	66.7 S	59.8	68.2 S	61.2	68.0
		64.4 P				
53.0	53.2	63.8 S	58.0	67.5 S	59.1	65.8
		60.7 P		(63.7) P		
54.0	51.1	54.8 P	55.4	63.3 S	57.0	64.2
				(58.4) P		
55.0	48.9	47.2 P	53.3	50.5 P	54.8	52.1
56.0	46.8	47.6 P	51.3	50.1 P	52.7	50.1
57.0	44.7	42.9 P	49.2	45.7 P	50.6	46.4
58.0	42.6	41.7 P	47.3	46.5 S	48.5	44.4
				(44.4) P		
59.0	40.5	41.8 P	45.1	43.4 P	46.4	43.5
60.0	38.3	38.8 P	43.0	41.1 P	44.2	42.2
61.0	36.1	36.9 P	40.4	38.5 P	42.0	33.1
62.0	33.9	33.2 P	38.3	35.8 P	39.7	32.5
63.0	31.8	45.0 L	36.3	(45.4) L	37.6	33.8
		34.6 P		(37.5) P		
64.0	29.7	28.0 P	34.2	30.7 P	35.4	31.2
65.0	27.7	25.5 P	32.3	28.2 P	33.4	28.3
66.0	25.7	23.5 S	30.1	25.8 S	31.4	25.0
		22.3 P				
67.0	23.7	15.6 M	28.4	28.5 L	29.4	22.8
				20.7 P		
68.0	21.8	15.5 M	26.2	(31.8) L	27.5	22.0
				20.4 P		
69.0	19.9	17.2 M	24.2	20.5 P	25.6	21.2
70.0	18.0	15.9 M	22.4	19.3 P	23.7	20.2

130 °K, and once with the ordinate expressed in brightness temperature. In the first case some computed optical depths reached very high and correspondingly uncertain values. In order to avoid prejudicing the values of V_x by use of a much too large Y_M in equation (5), we have arbitrarily reduced all $\tau > 3.0$ to $\tau = 3.0$ for the determination of V_x. This has influenced only the profiles at $l \geqslant 67°$. The two determinations were made at widely different times and with independent estimates of V_M. The results are shown in table 1, which is constructed as follows.

Column 1: longitude l.

Column 2: velocity V_c at the tangent point relative to the local standard of rest assuming the KMW rotation curve.

Column 3: V_x from equation (5) determined from the line profiles with the ordinate expressed as optical depth. Double entries correspond to different adopted values of V_M. The location of V_M in each case is indicated by the letters, which have the following meanings.

P = peak.
S = high shoulder or subsidiary peak.
L = low shoulder or top of a low extension.
M = integration carried to maximum permitted value $\tau = 3$, i.e. $V_M = V(\tau = 3)$.

Column 4: V_x calculated from model I, a model in which the line profiles expressed in optical depth are calculated for a galaxy in which the KMW rotation curve is valid and the hydrogen density and velocity dispersion are constant, the latter having the value $\sigma = 6$ km/sec. The essential assumptions upon which the models are based are summarized in table 3.

Column 5: V_x determined from the observed line profiles expressed in brightness temperature. The letters have the same meanings as in column 3. The values between parentheses were rejected when a unique value of V_x was required. When this was not the case both values were retained.

Column 6: V_x calculated from model VI, which is identical with model I except that the line profiles were expressed in terms of brightness temperature and the velocity dispersion was taken as a linear function of distance from the galactic centre,

$$\sigma = (7.5 - 0.2\,R)\ \text{km/sec}, \qquad (6)$$

R being expressed in kpc.

The values of V_x listed in columns 3 and 5 have been corrected for zero line error at longitudes $l = 31°.3$, $33°.3$ and $40°.3$ by increasing Y_M and each value of Y in equation (5) by an appropriate amount. In the case of column 5, this amount was just the zero line error determined from the requirement that the brightness temperatures nowhere be negative. The corrections to V_x were between +1 and +2 km/sec. The corrections to the values listed in column 3 were smaller due to the magnification of the upper parts of the profiles, which caused the increase in Y_M to become more important relative to the increase in the value of the sum.

4. Construction of models

Any observed set of line profiles in the galactic plane can be represented by a model in which the hydrogen is in circular motion around the galactic centre with a velocity $\Theta_c(R)$, which may be any continuous function of distance from the centre but which is everywhere greater than a certain limiting function $\Theta_m(R)$ and is consistent with the velocity of galactic rotation in the solar neighbourhood,

$$\Theta_c(R) \geqslant \Theta_m(R) \quad \text{and} \quad \Theta_c(10) = \Theta_0\,. \qquad (7)$$

A further condition on the model is that the velocity dispersion σ at each point be sufficiently small that the observed irregularities in the line profiles can be reproduced,

$$\sigma \leqslant \sigma_m\,. \qquad (8)$$

Only the limiting values $\Theta_m(R)$ and σ_m are determined by the observations. Given any function $\Theta_c(R)$ satisfying (7) and any distribution of values of $\sigma(R, \varphi)$ satisfying (8), where φ is galactocentric longitude, it is possible to determine a hydrogen density distribution $n_H(R, \varphi)$ which reproduces the observed profiles exactly. When $n_H(R, \varphi)$ is derived in this way, it will never be unique in the region $R < 10$ kpc because the heliocentric distance is a double valued function of radial velocity. Additional ambiguity will be introduced in any region in which the relation

$$\frac{\mathrm{d}}{\mathrm{d}R}\left(\frac{\Theta_c}{R}\right) < 0 \qquad (9)$$

is not valid.

In the broad class of models discussed in this section we have assumed that all gas motions are perpendicular to the galactic radii and are a function only of distance from the galactic centre. The effect of superposing a radial motion upon a given rotation curve $\Theta_c(R)$ will be to increase the maximum velocity observed in each direction. We can estimate the magnitude of this effect as follows.

Let the rotation curve in the region just outward from a tangent point located at a distance R_t from the galactic centre be represented by the approximation

$$\Theta_c(R) = \Theta_c(R_t) + \frac{d\Theta_c}{dR}(R-R_t), \tag{10}$$

and let the radial motion within this region be a constant Π. The increase in maximum velocity observed along the line of sight through the tangent point at R_t will be

$$\Delta V(\Pi) = [(\Theta')^2+\Pi^2]^{\frac{1}{2}}-\Theta', \tag{11}$$

where

$$\Theta' = \Theta_c - R\frac{d\Theta_c}{dR}, \tag{12}$$

all quantities being evaluated at R_t.

In case $(\Theta')^2 \gg \Pi^2$, equation (11) reduces to

$$\Delta V(\Pi) \approx \frac{\Pi^2}{2\Theta'}. \tag{13}$$

If Π is not constant, equation (11) will give an upper limit to the velocity shift if we substitute for Π the maximum value it attains within the region. Similarly, if equation (10) does not represent an adequate approximation to $\Theta_c(R)$, substitution in equation (12) of the largest value of the derivative will give an upper limit to ΔV.

Local irregularities in the dependence of Θ upon R, such as we have admitted in model VII, will lead to large fluctuations in the values of Θ'. In a region of solid-body rotation, where $\Theta' = 0$, equations (10) and (11) will no longer be valid as written. However, since these details, if real, will probably be local features not extending over wide ranges of galactocentric longitude, it appears more reasonable to substitute values of $\Theta_c(R)$ from a smooth rotation curve into equation (12) regardless of the details of the adopted relation. If we do this, Θ' will remain quite large in that part of the Galaxy considered here. Substituting values from the KMW rotation curve, we find that Θ' increases outward from a value of about 150 km/sec at $R = 4$ kpc, and equation (11) is valid for all cases of practical interest.

TABLE 2

Effect of galactic expansion upon observed maximum velocities

(1) R (kpc)	(2) $\Delta V_\odot$	(3) ΔV_E (km/sec)	(4) $\Delta\Theta_c$
4.0	+6.4	+6.2*	−12.6*
5.0	+6.1	+2.3	− 8.4
6.0	+5.6	+1.0	− 6.6
7.0	+5.0	+0.5	− 5.5
8.0	+4.2	+0.3	− 4.5
9.0	+3.1	+0.1	− 3.2

* +5.6 and −12.0 if we allow for the variation of Π with R.

As an example of the effect of expansion on a rotation curve derived from maximum velocities we have adjusted the KMW rotation curve for an assumed expansion law,

$$\Pi(R) = 7\left(\frac{R_0}{R}\right)^2 \text{ km/sec}, \tag{14}$$

a form suggested by KERR (1962). The results are shown in table 2, where column 1 gives the distance from the galactic centre, column 2 the expected increase in the observed velocity due to the outward motion of the local standard of rest $\Delta V_\odot$, column 3 the expected increase due to outward motion near the tangent point ΔV_E, and column 4 the total correction $\Delta\Theta_c$ which must be applied to the KMW rotation curve to achieve the same maximum velocities in the presence of expansion. We have assumed, in the first approximation,

$$\Delta\Theta_c = -\Delta V_\odot - \Delta V_E. \tag{15}$$

The value of ΔV_E at $R_t = 4.0$ kpc is somewhat too large due to the variation of Π with R. This can be corrected by substituting $\Pi(R_m)$ for $\Pi(R_t)$ in equation (11) where R_m is the radial coordinate of the point where the maximum velocity is observed,

$$R_m \approx R\left[1+\left(\frac{\Pi}{\Theta'}\right)^2\right]^{\frac{1}{2}}. \tag{16}$$

TABLE 3
Summary of models

(1) Model	(2) Θ_c	(3) n_H	(4) σ	(5) Ordinate	(6) Computation
I	KMW	U	U	τ	602A
II	KMW	CA+U	U	τ	602A
III	KMW	CA+U	U	τ	602A
IV	KMW	CA	U	τ	602A
V	S	NA	U		hand
VI	KMW	U	S	T_b	X1
VII	C	C	S	T_b	X1

Explanation of symbols

Columns 2–4:
KMW: the rotation curve of KWEE, MULLER and WESTERHOUT (1954).
U : a constant (i.e. uniform).
S : a smooth function of galactocentric distance R (e.g. KMW).
C : any function of R alone (i.e. circular).
CA : circular arms.
NA : non-circular arms.

Column 6:
602A: IBM 602A Calculating Punch Machine.
X1 : Electrologica X1 computer.

All quantities on the right in equation (16) are evaluated at $R = R_t$. Even in the present case, where Π is quite a steep function of R, the required correction is small. In view of the lack of reliable evidence on radial motion in the region of the Galaxy considered here, we have chosen to assume that for the gas $\Pi(R) \equiv 0$. However, it should be borne in mind that shifts in the observed rotation curve of the order of those shown in column 3 of table 2 may well occur as a result of general radial motion and that local disturbances of about the same magnitude could result from local gas motions in the radial direction.

In addition to the assumption of no radial motion, we have also assumed in all models that Θ_c is a function of distance from the galactic centre only. Streaming in the tangential direction corresponds to failure of this assumption and will influence the line profiles strongly, as discussed in section 3. A model in which tangential streaming is important will be discussed briefly in section 5.

The velocity smoothing parameter $\sigma(R, \varphi)$ is used to represent the combined effect of thermal and turbulent broadening and possible unresolved streaming motions. It has been determined by considering the steepness of the terminations of the line profiles, where we anticipate that an unsmoothed line profile will drop abruptly to zero from a high value at the maximum permitted velocity. We note that many features in the line profiles appear sharper than these terminal drops. This can be attributed to the very large volume of space that contributes to those parts of the profiles near their terminations. Here the length of the truncated cone within which the observed material lies reaches a pronounced maximum, so that just in this part of the profile the largest-scale streaming effects will remain unresolved. The sharpest features observed in the profiles presumably originate in the neighbourhood of the Sun where the spatial resolution is greatest. As we are concerned here only with the kinematics near the tangent points, we have tried to represent by σ all motions which are unresolved in the tangent region. The fact that smaller-scale motions may be resolved in other regions has not concerned us.

In table 3 we have summarized the properties of the models considered in this section. The model number is given in column 1. Columns 2–4 contain specifications of the adopted rotation curve, density distribution and velocity dispersion, respectively. Column 5 indicates the form in which the line profiles were represented, optical depth (τ) or brightness temperature (T_b), and column 6 shows the method of computation.

The KMW rotation curve as well as our model V is based upon the concurrent assumptions that the hydrogen density at some, but not all places along the locus of tangent points is comparable with the density elsewhere, and that the velocity curve $\Theta_c(R)$ is a smooth

function of R. This has led to a model comprising two well-defined spiral arms with very low density elsewhere. The Kootwijk map of the Galaxy (SCHMIDT, 1957) shows the resulting run of hydrogen density along the locus of tangent points. We have adopted an idealized version of this picture as the basis of our first set of models.

4.1. *Models I–IV: Some simple models*

In order to examine the effect on the line profiles of the concentration of hydrogen into well-defined arms, we have constructed models I–IV in which we have assumed such concentration to varying degrees. In all models we have assumed the KMW rotation curve and a uniform velocity dispersion, derived from a preliminary investigation, of $\sigma = 6$ km/sec, a value rather smaller than suggested by KMW. This reduction in σ may be the result of the improved resolution of the Dwingeloo telescope and the narrower bandwidth of the receiver. The assumed density distribution in model I was uniform. In model IV all the hydrogen was assumed concentrated in two rings, one with inner and outer radii of 5.5 and 6.0 kpc respectively and the other with radii 7.5 and 8.0 kpc. The densities within these two rings were assumed uniform and equal. The assumption that the hydrogen is distributed in rings is, of course, not realistic, but it has been adopted in most of the models that we have discussed as a reasonable approximation to the structure over small sectors near the tangent points. The approximation fails seriously when the maximum velocities are defined by hydrogen located at considerable distances from the tangent points, as in the case of model IV.

Models II and III are intermediate cases, in which two rings of high density are defined as in model IV but the remainder of the plane is filled with hydrogen with a density respectively 0.4 times and 0.1 times that in the rings. No figures have been assigned to the hydrogen densities in models I–IV, since only the relative densities between arm and background are important. The ordinates of the line profiles are optical depths, which will be proportional to hydrogen density if the excitation temperature is uniform, so that a change in density will result only in a corresponding change in scale of the ordinate of the line profiles. Since these must be scaled in any case to match the observed line profiles, the density need not be determined directly. The terminal velocities V_x determined from optical depth profiles will be independent of the assumed density.

The line profiles and terminal velocities for 50 longitudes corresponding to the observed points were calculated on the basis of models I–IV using an IBM 602A Calculating Punch Machine and associated equipment formerly installed at the Leiden Observatory. The computations were carried out as follows.

1) For each longitude a table was constructed giving velocity with respect to the local standard of rest as a function of galactocentric distance R,

$$V = \left[\frac{R_0}{R}\,\Theta_c(R) - \Theta_0\right] \sin l\,. \tag{17}$$

2) Interpolation in this table gave R for whole values of V in km/sec,

$$R = R(V)\,. \tag{18}$$

Corresponding values of D, the distance from the tangent point, were calculated:

$$D(R) = (R^2 - R_t^2)^{\frac{1}{2}}\,, \tag{19}$$

where $D(R) \equiv 0$ for $R \leqslant R_t$.

3) The optical depth in each interval of 1 km/sec in the unsmoothed line profile $\tau_0(V)$ was set equal to the length of the corresponding interval in D multiplied by a weighting factor representing the mean hydrogen density within the corresponding interval along the line of sight, so that

$$\tau_0 \propto \int_{D_1}^{D_2} n_H[(R_t^2 + D^2)^{\frac{1}{2}}]\,\mathrm{d}D\,, \tag{20}$$

where the density distribution $n_H(R)$ has been described above. For model I we have taken

$$n_H(R > 10\ \mathrm{kpc}) = \tfrac{1}{2} n_H(R < 10\ \mathrm{kpc}) \tag{21}$$

to compensate for the fact that the line of sight extends in only one direction from the Sun. This refinement, which appeared to be unimportant even for the highest longitudes, was abandoned in the computation of later models. Steps 3) and 4) were carried out for models I and IV only.

4) The line profiles computed as in 3) were smoothed

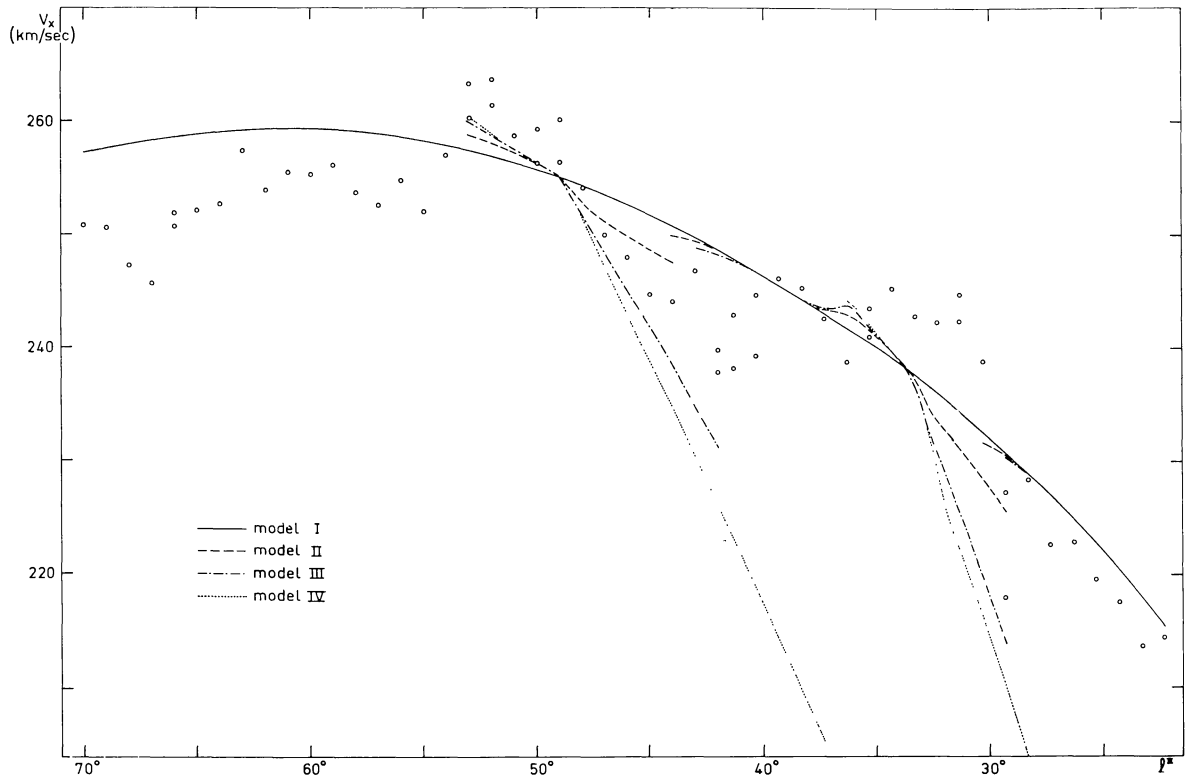

Figure 8. Observed and computed values of the terminal velocity for models I–IV. The ordinate is the terminal velocity V_x computed by means of equation (5) from the observed or computed optical depth profiles and expressed with respect to the galactic standard of rest. The open circles represent the observations, and the solid and broken curves represent models I–IV. The abscissa is the longitude of observation, which is shown increasing to the left, as it appears in the sky. Thus the abscissa is reversed with respect to that adopted for figures 1, 2, and 12, where the galactocentric distance is shown increasing to the right.

by an approximation to a Gaussian function with a dispersion $\sigma = 6$ km/sec,

$$\tau(V) = \sum_{n=1}^{23} [\tau_0(V+\tfrac{1}{2}-n) + \tau_0(V-\tfrac{1}{2}+n)]G_6(n), \quad (22)$$

where

$$G_6(n) = \frac{30.95\, G_6(n-1)}{29.67 + n}, \quad n \geqslant 2, \quad (23)$$

$G_6(1)$ being a suitable normalizing factor.

5) The profiles for models II and III were calculated by combining those of models I and IV in such proportions as to keep the maximum densities constant.

6) The terminal velocities V_x were calculated for all profiles. For some profiles two values were calculated corresponding to two different adopted values of V_M chosen as described in section 3.

The results of these calculations are shown in figures 8 and 9. Figure 8 shows the terminal velocities V_x expressed, for convenience, with respect to the galactic standard of rest,

$$V_{g.s.r.} = V_{l.s.r.} + \Theta_0 \sin l. \quad (24)$$

The points are determined from the observed line profiles expressed in optical depths, as in column 3 of table 1, and the curves are derived as described above from models I–IV. The run of observed points shows some of the same characteristics as did the KMW observations. In particular, the peaks at $l = 31°$ and 52° are still the most prominent features. The deviations from a smooth curve are about the same as those found by KMW, ± 7 km/sec. The most noticeable differences are that the clear stepwise trend in the KMW observations is here replaced by a more undulating appearance, and that the observed terminal velocities frequently fall above the calculated values. If one were

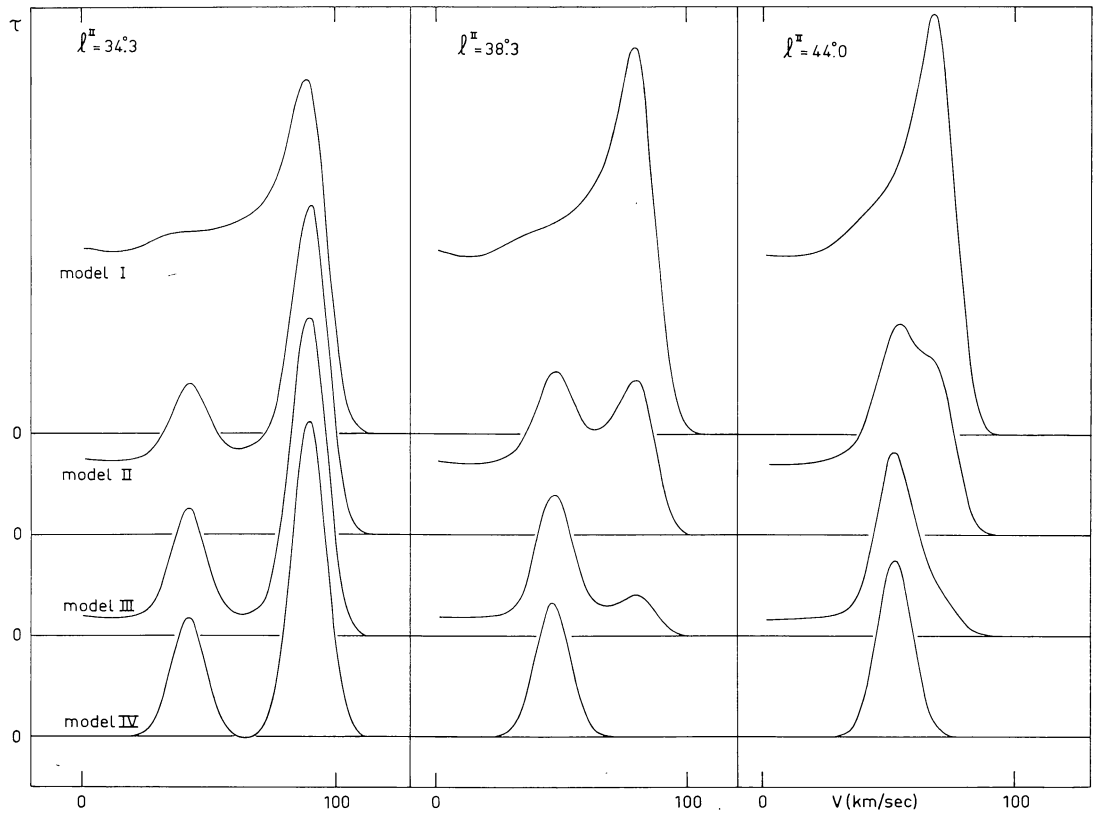

Figure 9. Line profiles calculated from models I–IV at three longitudes. The abscissa is velocity with respect to the local standard of rest. The ordinate is optical depth in arbitrary units. The optical depth will be proportional to the adopted scale of the hydrogen density.

to base a rotation curve upon the upper envelope of these observed velocities, following the method of KMW, one would derive rotational velocities 3 to 4 km/sec greater than theirs. That this difference is too great to be accounted for by systematic differences in the choice of V_M, which was implicitly made by KMW in their selection of the part of the line profile to be represented by the model, is illustrated by the fact that selecting the lower of the two observed points, where present, does not go far toward reducing the observed peaks to the level of the curve computed from the uniform model. It is possible that this difference is the result of the greater resolution of the present observations both in frequency and position. This will result in less smooth line profiles and we will tend to reject from the descending branches peaks which in our line profiles lie clearly short of the maximum velocities. Observations with lower resolution will tend to smooth such multiple peaks together into single features at correspondingly lower velocities and with greater velocity dispersions, in agreement with the differences which we have noted.

The computed curves show a stepwise behaviour far more clearly than the observations, but the shapes are not so different as to make quantitive comparison impossible. In the region of the outer ring the computations match the observations reasonably well for some model between II and III, provided we imagine the computed curves raised about 3 km/sec. The inner ring appears to have been placed too far outward, the computed maximum velocities occurring at $l = 36°$ instead of $l = 32°$ as shown by the observations, which corresponds to a position of the ring at 5.0 to 5.5 kpc from the galactic centre. Supposing this alteration made and all computed velocities increased, this time by about 5 km/sec, model III seems to fit the observations reasonably well.

In the regions not influenced by the rings, the models

are less satisfactory. At $l > 53°$, models I–III are represented by the solid curve, which is systematically too high, while model IV is undefined. Clearly the models are inadequate in this region. Between the rings, none of the models represents the near constancy of V_x with l between 32° and 42°, even taking into account a possible inward shift of the inner ring. Inward from 30° the measured values fall systematically below model I, but if we suppose all computed velocities increased and the inner ring moved inward they may fall between models II and III.

In figure 9 we have reproduced the computed line profiles for models I–IV at three typical longitudes. At $l = 34°.3$ the tangent point lies at $R = 5.6$ kpc, in the inner ring of high density. Here the high-velocity cutoff of the profile is little affected by the choice of model, although the outer ring is prominent at lower velocities in models II–IV. At $l = 38°.3$ the tangent point lies just outside the inner ring, at $R = 6.2$ kpc. Here models II and III show a pronounced peak due to the presence of low-density material near the tangent point. The $V_x(l)$ relation will show little deviation from the relation for uniform density as long as the outermost peak is adopted as V_M. In order that the second peak be chosen, the first must be less prominent than that shown for model III. The only observed profile that resembles model III at $l = 38°.3$ is the one at $l = 63°.0$. At $l = 44°.0$ the tangent point lies at $R = 7.0$ kpc, somewhat inside the outer ring. The secondary peaks in models II and III have partly merged with the peak arising in the ring, and the computed line profiles show only shoulders. The profile from model II resembles a number of observed profiles in this longitude range. The choice between the position of the shoulder and of the peak for V_M results in two values of V_x for model II at this longitude.

We cannot expect the observations to show such a clear-cut pattern as that derived from the models, but if the irregular dependence of V_x upon l is primarily due to density fluctuations, we can expect some general resemblance between some model in the range I–IV and the observations. We have considered the following arguments in trying to decide where in this range a suitable model should lie.

1) In order to achieve sufficient deviation from the smooth run of $V_x(l)$ predicted by model I, the background density must be below about 40 per cent of the ring density, thus between the model II and model III values, or possibly lower.

2) As soon as the background density reaches this level, the departures of V_x from the model I values are sufficient that they must be strongly influenced by the hydrogen distribution at considerable distances from the tangent points. When this occurs, the magnitudes of the departures from the model I curve will be reduced by the tilt of the spiral arms, as compared with the curves derived here for circular models. This will require a further decrease in background density, probably at least to the 10 per cent level.

3) Model III predicts line profiles at many longitudes with low secondary peaks at high velocities, such as we observe only at $l = 63°.0$. In order to reduce these peaks to insignificance we must reduce the background density still further. The example $l = 38°.3$ of model III shown in figure 9 implies that the background density must be reduced by at least a factor 10 to less than 1 per cent of the ring density before the secondary peak will no longer be clearly visible. Substituting spiral arms for the rings will not influence the height of the secondary peak, but it will bring the main peak somewhat closer and thereby make the secondary peak less prominent. It should nevertheless be visible as a low extension at many longitudes.

We conclude from the above arguments that if the Galaxy can be represented at all by a model of this type, it must be one with well-defined spiral arms, not circular arms as assumed in models II–IV, and with a very low background density of hydrogen. Only in this way can we explain the run of V_x with l and the absence of low-intensity extensions at the high-velocity terminations of the line profiles without abandoning our assumption of a smooth rotation curve. Model V is based on these considerations.

4.2. *Model V: A smooth rotation curve*

We have used in model V a rotation curve derived from the KMW curve by addition of a smooth function so chosen that the circular velocity at $R = 10$ kpc remains unchanged while the velocities at $R = 7.9$ and 5.4 kpc are increased sufficiently that no measured value of V_x lies significantly above the value predicted from a calculation similar to that made for model I,

$$\Theta_V = \Theta_{KMW} - 1.85 + 3.145R - 0.296R^2, \quad (25)$$

where R is expressed in kpc. This revised rotation curve yields a value of $AR_0 = 164$ km/sec. The function $\Theta_V(R)$ is tabulated in column 3 of table 5 and is plotted in figure 12.

In model V we assume further a velocity dispersion $\sigma = 6$ km/sec and a density distribution in which all the neutral hydrogen is concentrated in arms whose shapes may be irregular but which generally follow the pattern of a winding spiral. The values of V_x calculated from model I where modified in the same way as the KMW rotation curve to obtain a new set appropriate to model V. Necessarily these values are almost all greater than the observed values listed in column 3 of table 1. The differences between the observed and computed values

$$V_D = V_x(\text{col. 4}) - V_x(\text{col. 3}) + \Theta_V - \Theta_{KMW} \quad (26)$$

were interpreted as resulting from the departures of the hydrogen concentration from the tangent points. We have assumed that the difference between the maximum projected velocity of the hydrogen in the line of sight and the observed value of V_x is independent of the point at which this hydrogen is located. This is equivalent to the assumption that the end of the line profile will not be altered in form if hydrogen is absent from the tangent region, but only shifted to a lower velocity. This is not strictly true, but it serves to permit a reasonable estimate of the location of the hydrogen. The velocity discrepancy V_D will thus be related to the distance along the line of sight between the tangent point and the hydrogen with the highest velocity and thus the smallest distance from the tangent point.

The relation between velocity discrepancy V_D and distance from the tangent point D can be expressed by defining an angle φ' where

$$D = R_t \tan \phi' . \quad (27)$$

We can then write

$$1 - \cos \phi' = \frac{V_D}{\Theta - \frac{d\Theta}{dR} R_t} K , \quad (28)$$

where K is a correction factor which in all cases considered here takes a value between 0.95 and 1.00. The expression for K in terms of the second derivative of Θ is

$$K = 1 + \frac{V_D R_t^2 \frac{d^2\Theta}{dR^2}}{2\left(\Theta - R_t \frac{d\Theta}{dR} - V_D\right)\left(\Theta - R_t \frac{d\Theta}{dR}\right)} . \quad (29)$$

Here Θ and its derivatives are evaluated at R_t.

Values of D have been determined corresponding to the observed values of V_x in column 3 of table 1. In the few cases where $V_D < 0$, we have set $D = 0$. As expected, D reaches zero in the directions where we suppose that the tangent point lies in an arm. Elsewhere D climbs to values almost as large as 3 kpc. We expect that it will oscillate between zero and large values as R_t increases, corresponding to the passage from one arm to the next. Thus the increasing branch will correspond to points on the outer edge of an inner spiral arm, the maximum to the direction in which the outer edge of the inner arm and the inner edge of the next outer arm are equally far from the tangent point along the line of sight, and the subsequent decrease to the convergence of the inner edge of the outer spiral arm towards the locus of tangent points. A flat minimum will correspond to a broad arm and a sharp one to a narrow arm, although the appearance of the minima can be strongly effected by the assumed local values of $\Theta_c(R)$.

The observed run of D with l satisfies these expectations quite closely, and we have been able to draw an incomplete map of the edges of the spiral arms. This map is shown in figure 10, where we have assumed that the arms are winding spirals. A similar map could be drawn, based on the contrary assumption. Two arms labelled B and C are shown clearly, and there are traces of two others. The fragment called A might be an inward extension of arm B, as shown by the broken line. The most remote part of arm C seems to be observed at the same longitudes as the nearest part of arm B. These two features are identified with the two values of V_x consistently observed at longitudes around $l = 41°$. The edges of the arms are shown by solid lines or, in cases of uncertainty, by broken lines. The region of the arm itself is shown by shading. Arm B appears to be rather broad near the tangent point as the inner and outer edges are widely separated. Arm C must be narrower as the inner and outer edges almost run together at the tangent point.

The tilts of the inner and outer arms, neglecting the uncertain extensions at the far ends of both, are 76°.5

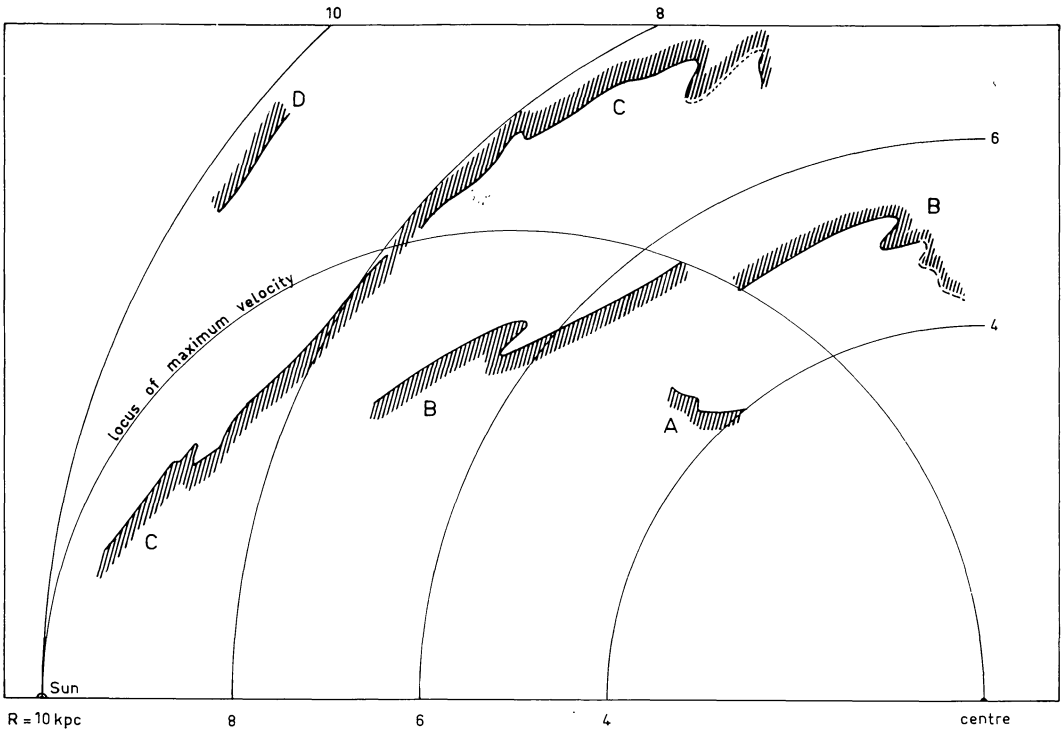

Figure 10. Edges of the spiral arms according to model V. The edges of the arms are shown as solid or, in case of ambiguity, broken lines. The location of the arms themselves is shown by shading. This map is based upon the assumption that the arms are trailing. The corresponding map for the assumption of leading arms may be obtained by reflecting each point in the diagram along the line of sight to the opposite side of the locus of maximum velocity.

and 78°.1 respectively. These values lie between the corresponding values derived from the KMW data and the value of about 84° expected from the model of a two-armed spiral and derived by SCHMIDT (1957) and by KARDASHEV *et al.* (1964). Figure 10 gives an exaggerated impression of the difference in tilt between the arms because of the greater thickness of arm B.

The primary drawback to this picture of the Galaxy is that the whole inter-arm region must be virtually free from neutral hydrogen. In view of the appearance of other galaxies this seems a very implausible result, and we have devoted some effort to a test for the presence of low-density hydrogen between the arms.

4.3. *Model VI: Search for inter-arm hydrogen*

In this section we shall examine the line profiles more closely with the aim of detecting the influence of any neutral hydrogen in the region between the arms postulated in section 4.2. Such hydrogen should manifest itself through the presence of some form of low extensions to those line profiles whose terminal velocities V_x are low compared with the values expected on the basis of a smooth rotation curve. This difference was measured in the preceding section by the velocity discrepancy V_D. In this section we have considered the line profiles expressed in brightness temperature and have consequently used V_x from column 5 of table 1. These measured values must be compared with values computed from a model based upon a smooth rotation curve and a uniform hydrogen distribution. We have constructed model VI for this purpose.

For model VI we have adopted the KMW rotation curve and the random velocity distribution defined by equation (6) rather than the constant value used in earlier models. Since the line profiles were to be expressed in terms of brightness temperature, it was necessary to specify values of the hydrogen density and the excitation temperature. The latter was assumed to be 130 °K, while for the former a general average of the model VII results, $n_H = 0.28$ atoms $\cdot$ cm^{-3}, was adopted. From this model, using the method to be

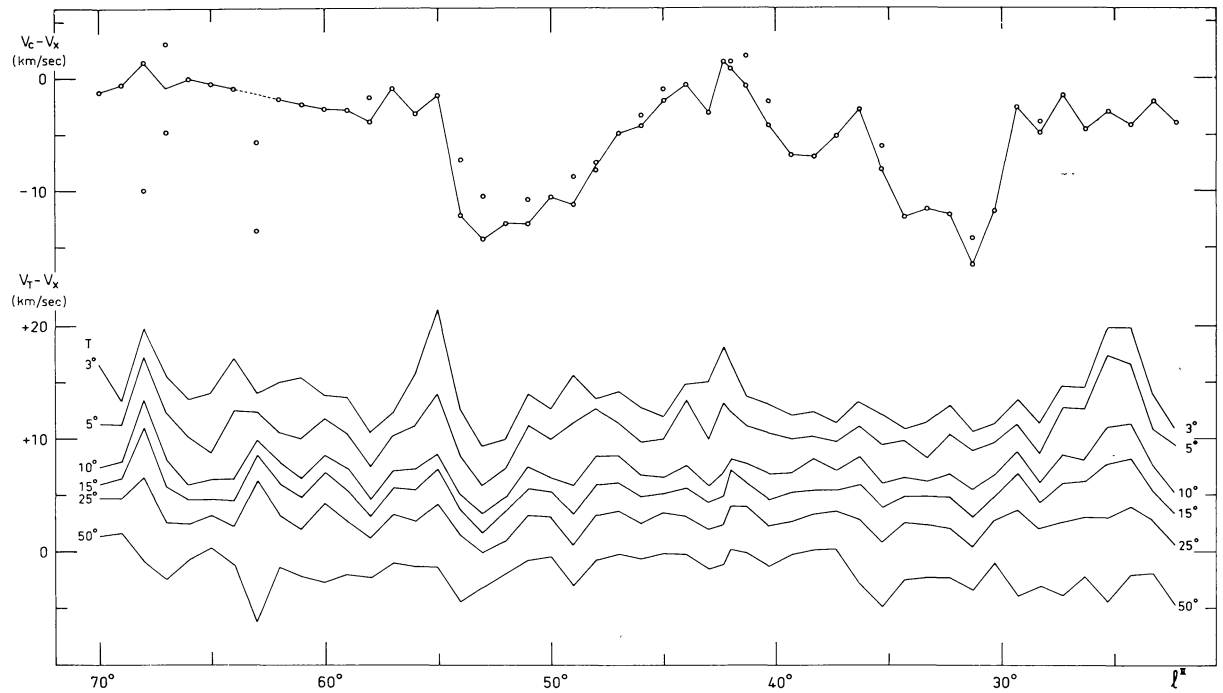

Figure 11. Search for low extensions to line profiles. The upper curve shows the discrepancy between the measured terminal velocity and the maximum velocity expected from a smooth rotation curve. The lower curves show the run of differences between the velocity at which each line profile reaches the brightness temperature T and the measured terminal velocity. The presence of low-density hydrogen between the arms shown in figure 10 should cause the first curves of the lower group to follow the run of the upper curve to some extent.

described in section 4.4, line profiles of the form $T_b(V)$ were computed and the corresponding values of V_x were determined. This was done at intervals of 5° in longitude; values for the intervening longitudes were interpolated by comparing the calculated values of V_x with the values of V_c tabulated in column 2 of table 1, which also pertain to the KMW rotation curve, and interpolating in the difference $V_x - V_c$. The resulting values of V_x for model VI are shown in column 6 of table 1.

It might be argued that the model V rotation curve is more appropriate to the problem at hand than the KMW curve. The latter was chosen for this calculation as being representative of the observations at a greater number of longitudes than the former, which is based essentially upon only two observed points in addition to the solar neighbourhood. Since the difference between the two curves changes only slowly with longitude, the behaviour of the differences in V_x, which is what concerns us here, will not depend in an important way upon which rotation curve is chosen. Addition of a constant term to the calculated values of V_x will have no influence upon the results derived in this section.

Finally we have chosen to measure the velocity discrepancy by the difference $V_c - V_x$, where V_c and V_x were taken from table 1, columns 2 and 5 respectively. Since V_x calculated from model VI exceeds V_c for the KMW curve by a nearly constant amount, the use of V_c will introduce an essentially constant term into the velocity discrepancy.

The difference $V_c - V_x$ is plotted as a function of longitude in the upper part of figure 11. The points corresponding to all measured values of V_x are plotted as open circles. Since it was necessary for the following analysis to determine a unique value of $V_c - V_x$ at each longitude, we have selected preferred values of V_x as described in section 3, and the solid line passes through the corresponding points. At two longitudes we have chosen mean values, and the point at $l = 63°$ has been omitted because of the strongly distorted appearance of the line profile. In the two minima, corresponding

to the directions in which the arms postulated in model V cross the semi-circle of tangent points, the difference $V_c - V_x$ reaches about -13 km/sec, the negative value being due in part to the use of the KMW rotation curve in place of that derived from model V and in part to the use of V_c in place of the calculated values of V_x. The maxima of the curve, corresponding to the inter-arm regions, attain slightly positive values.

In order to investigate the observed line profiles for possible extensions at low intensity, we have read off the velocities at which each profile first reaches each of six values of the ordinate, $T = 3°$, $5°$, $10°$, $15°$, $25°$, and $50°$. We designate these velocities $V_T(l)$. In the lower part of figure 11 we have plotted $V_T - V_x$ for each value of T. The values of V_x adopted were the same as those upon which we based the continuous line in the upper part of the figure. The points at $l = 63°$ are plotted but are excluded from the further analysis.

If the variation in $V_c - V_x$ is due to an irregular density distribution, we should expect residual hydrogen between the arms to result in low-intensity extensions to the line profiles, causing V_T for small T to follow a run more similar to that of V_c than to that of V_x. This would result in the upper of the $V_T - V_x$ curves tending to reflect the behaviour of the $V_c - V_x$ curve. The lower curves of the lower group should show less variation. The value of T at which the variation ceases to follow that of $V_c - V_x$ should measure the mean hydrogen density in the inter-arm region. Judging from the results shown in figure 9, we estimate that an inter-arm density of 1 per cent of the arm density would influence only $V_3 - V_x$, while an inter-arm density of 10 per cent would influence all exept $V_{50} - V_x$. If all the lower curves are independent of the upper one, we must conclude either that the background density is normally less than 1 per cent of the arm density or that there are real irregularities in the galactic rotation curve for neutral hydrogen.

Figure 11 shows very little tendency for the $V_T - V_x$ curves to follow the $V_c - V_x$ curve. The most prominent feature that is common to both is the peak at $l = 55°$. But whereas the $V_c - V_x$ curve remains high at $l > 55°$, the $V_T - V_x$ curves drop back quickly to about their mean level. An examination of the profiles in this region suggests that the extension at low intensity at $l = 55°$ may be due to the presence in the line of sight of some of the hydrogen that is causing the high value of V_x at lower longitudes. At higher values of l this hydrogen is no longer visible.

TABLE 4

Test for low-intensity extensions to line profiles

(1) T (°K)	(2) x_T	(3) m_x	(4) x_T (corrected)
3	+0.313	±0.071	+0.118
5	+0.237	±0.062	+0.018
10	+0.176	±0.047	−0.055
15	+0.177	±0.040	−0.040
25	+0.153	±0.032	−0.052
50	+0.108	±0.045	−0.047

In order to estimate quantitatively the relation between the curves in figure 11, we have supposed that there exists a relation of the form

$$V_T - V_x = x_T(V_c - V_x) + y_T \qquad (30)$$

between each $V_T - V_x$ curve and the $V_c - V_x$ curve. We have solved these sets of condition equations by least squares for x_T and y_T at each value of T using all longitudes except $l = 63°$. The results are shown in table 4, where the value of T is given in column 1, the corresponding value of x_T in column 2 and its mean error in column 3. Clearly any shift in the height of the adopted rotation curve, such as results from our use of V_c in place of the values of V_x from column 6 of table 1, will be absorbed in the derived values of y_T. The same may be said for most alternative rotation curves that might have been adopted, provided they remain smooth.

For a galaxy with a smooth rotation curve and sharply defined arms, we expect the values of x_T to decrease from about 1.0 in the first line to about 0.0 in the last line. The larger values will be reduced somewhat by the low intensity of the extension. Thus a point at level T will be displaced by smoothing to a higher velocity with respect to V_c if the density at the tangent point is high than if it is low. The magnitude of this effect cannot be estimated in the absence of a specific model. The disappearance of the correlation of x_T with T will be equivalent with the disappearance of a low-intensity extension under the wing of the main profile. A comparison of the amplitude of variation of $V_c - V_x$, about 15 km/sec, with the assumed velocity dispersion of about 6 km/sec indicates that it is not

likely that the correlation will be greatly reduced by this effect.

A model in which the irregularities in the $V_c - V_x$ curve are the result of corresponding behaviour of the relation $\Theta_c(R)$ leads us to expect values of x_T in the neighbourhood of zero, with no pronounced dependence upon T. The effect of overlapping of streams corresponding to different values of Θ_c within the antenna beam leads us to expect some slightly positive values of x_T for small T, but the calculation of this effect requires more elaborate models than we are at present in a position to construct.

We can correct approximately for two systematic effects which will influence the values of x_T. In the first place, the adopted values of V_x will be subject to random errors, and these will introduce a spurious correlation between $V_c - V_x$ and $V_T - V_x$. If the root-mean-square error in V_x is $\Delta_1 V_x$, then the systematic effect can be removed by subtracting $n(\Delta_1 V_x)^2$ from the coefficients $\Sigma(V_c - V_x)^2$ and $\Sigma(V_c - V_x)(V_T - V_x)$ in the normal equations, where n is the number of condition equations. In the second place, each value of V_T will depend upon the height of the peak from which it is derived as well as upon the position of the peak. Let the mean height of the peaks be T_0. The velocity shift at the level T due to a change of peak height from T_0 to $T_0 + \Delta T$ will be

$$\Delta_2 V = \frac{\sigma\sqrt{2}}{T_0}\left(\ln\frac{T_0}{T}\right)^{-\frac{1}{2}}\Delta T. \qquad (31)$$

If a correlation exists between the heights of the peaks and $V_c - V_x$, then the corresponding shift in V_T, $\Delta_2 V$, will introduce a spurious correlation between $V_T - V_x$ and $V_c - V_x$. If the second model suggested above is valid, as the values of x_T in column 2 of table 4 indicate, then the appropriate value of ΔT to select at each longitude is

$$\Delta T = T(V_M) - \langle T(V_M)\rangle, \qquad (32)$$

where the average $\langle T(V_M)\rangle$ is taken over all longitudes considered. In the case of the first model, the appropriate value of ΔT can not easily be determined as we can not, in practice, identify the extensions to the line profiles for which we are testing. We have therefore used the values of T at V_M and looked for a correlation between these and the values of $V_c - V_x$ by solving by least squares for the coefficient α in the 49 condition equations of the form

$$T(V_M) = \alpha(V_c - V_x) + \beta. \qquad (33)$$

We found $\alpha = +1.63 \pm 1.04$ °K · sec · km^{-2} indicating that a significant correlation exists. The corresponding dependence of x_T upon $(V_c - V_x)$ may be estimated by substituting in equation (31)

$$\Delta T = \alpha\Delta(V_c - V_x), \qquad (34)$$

so that a contribution to x_T,

$$\Delta_2 x_T = \frac{\Delta_2 V}{\Delta(V_c - V_x)} = \frac{\alpha\sigma\sqrt{2}}{T_0}\left(\ln\frac{T_0}{T}\right)^{-\frac{1}{2}}, \qquad (35)$$

may be expected. Substituting here for T_0, which is the mean value of $T(V_M)$, $T_0 = 93.4$ °K, and for α and σ, we can determine $\Delta_2 x_T$ as a function of T.

Recomputing x_T under the assumption $\Delta_1 V = 2.5$ km/sec and subtracting the expected effect of correlation with profile height $\Delta_2 x_T$, we find the values of x_T listed in column 4 of table 4. The clustering of these values around zero must be in part fortuitous, as x_T is quite sensitive to the assumed value of $\Delta_1 V$ and the $\Delta_1 V$ correction reduces all the values of x_T while the ΔT correction partly counteracts this trend, so that a relatively small change in $\Delta_1 V$ can have a large effect. The value 2.5 km/sec was estimated from the differences arising from different adopted values of V_M and from small-scale irregularities in the run of $V_c - V_x$ with l. The mean errors listed in column 3 remain roughly applicable to the results in column 4, but we must also admit the possibility of systematic errors of at least the same magnitude entering through the applied corrections. Despite these uncertainties, the results shown in table 4 indicate that unless we are prepared to accept a galactic model in which the hydrogen density in the spiral arms exceeds that elsewhere by at least a factor of 100 and in which regions of intermediate density are rare, we must consider a model in which the observed irregularities in the run of the terminal velocities reflect corresponding irregularities in the behaviour of the rotation curve $\Theta_c(R)$. This consideration has led us to construct model VII.

4.4. *Model VII: An irregular rotation curve*

It is suggested by the arguments given above that the hydrogen density does not commonly vary over a wide

TABLE 5

Parameters used in model computations

(1)	(2)	(3)	(4)	(5)	(1)	(2)	(3)	(4)	(5)
R (kpc)		$\Theta_c(R)$ (km/sec)		$n_H(R)$ (cm^{-3})	R (kpc)		$\Theta_c(R)$ (km/sec)		$n_H(R)$ (cm^{-3})
	KMW	Model V	Model VII	Model VII		KMW	Model V	Model VII	Model VII
3.8	211.4	217.2	208.7	0.23	7.0	246.7	252.4	243.3	0.24
3.9	212.9	218.8	210.5	0.25	7.1	247.5	253.1	244.0	0.30
					7.2	248.2	253.6	245.4	0.36
4.0	214.4	220.4	212.3	0.31	7.3	248.9	254.2	246.9	0.38
4.1	215.9	222.2	215.1	0.32	7.4	249.6	254.8	248.6	0.36
4.2	217.4	223.5	218.1	0.25					
4.3	218.9	225.1	221.0	0.12	7.5	250.3	255.4	250.7	0.33
4.4	220.3	226.5	223.9	0.12	7.6	250.9	255.9	253.5	0.25
					7.7	251.4	256.2	256.0	0.21
4.5	221.7	228.0	225.8	0.12	7.8	251.9	256.6	258.8	0.30
4.6	223.0	229.4	226.8	0.14	7.9	252.4	256.9	258.5	0.32
4.7	224.2	230.6	225.7	0.16					
4.8	225.4	231.8	228.3	0.17	8.0	252.9	257.3	258.1	0.32
4.9	226.6	233.1	229.6	0.13	8.1	253.3	257.5	260.5	0.22
					8.2	253.7	257.7	257.0	0.10
5.0	227.8	234.3	229.8	0.06	8.3	254.1	258.0	254.0	0.20
5.1	229.0	235.5	237.0	0.15	8.4	254.4	258.1	251.5	0.20
5.2	230.2	236.7	240.1	0.35					
5.3	231.4	237.9	239.7	0.42	8.5	254.7	258.2	249.2	0.33
5.4	232.5	239.0	238.6	0.41	8.6	254.9	258.2	251.3	0.29
					8.7	254.9	258.0	253.5	0.17
5.5	233.6	240.1	238.5	0.40	8.8	254.8	257.7	253.9	0.15
5.6	234.6	241.1	240.0	0.25	8.9	254.6	257.3	252.4	0.21
5.7	235.5	242.0	242.4	0.30					
5.8	236.4	242.8	241.4	0.26	9.0	254.4	256.9	250.7	0.31
5.9	237.3	243.7	236.1	0.19	9.1	254.2	256.5	248.6	0.38
					9.2	253.9	255.9	247.9	0.20
6.0	238.2	244.6	236.1	0.18	9.3	253.5	255.3	250.0	0.20
6.1	239.1	245.4	238.6	0.29	9.4	253.0	254.6	251.0	0.20
6.2	240.0	246.3	242.4	0.37					
6.3	240.9	247.1	243.3	0.38	9.5	252.5	253.8	251.5	0.20
6.4	241.7	247.8	243.0	0.49	9.6	252.0	253.1	251.5	0.40
					9.7	251.5	252.3	251.5	0.60
6.5	242.6	248.7	240.4	0.51	9.8	251.0	251.6	251.0	0.80
6.6	243.5	249.5	237.6	0.36	9.9	250.5	250.8	250.5	0.70
6.7	244.3	250.2	239.5	0.30					
6.8	245.1	250.9	240.6	0.25	10.0	250.0	250.0	250.0	0.60
6.9	245.9	251.7	242.7	0.22					

range from one large region of the Galaxy to another, as between the arms and the inter-arm regions. If such variations, by a factor of 20 or more, were common we would expect to see in many directions line profiles with low extensions, and we have seen that these are rarely found. Some special kinematical behaviour might conceal such an effect. One might, for example, postulate the existence of gas streams associated with the spiral arms. Models of this type will be discussed briefly in section 5.

Supposing that there are no large regions of very low hydrogen density and that the angular velocity everywhere decreases outward, there will be, in the neighbourhood of each tangent point, enough hydrogen to determine the behaviour of the corresponding line profile near its termination. This argument makes it plausible to adopt a circularly symmetric galactic model for the calculation of line profiles, since such a model should provide a reasonable approximation to the real pattern of hydrogen density and motion in a very restricted region about the locus of tangent points. The assumption that the hydrogen is located in galactocentric arcs over this small range of distance is not a severe restriction. The main purpose of including density variations at all in this model is to provide for the matching of the ordinates of the computed line profiles to the observations. This same end was achieved by KMW by normalizing their observations to standard

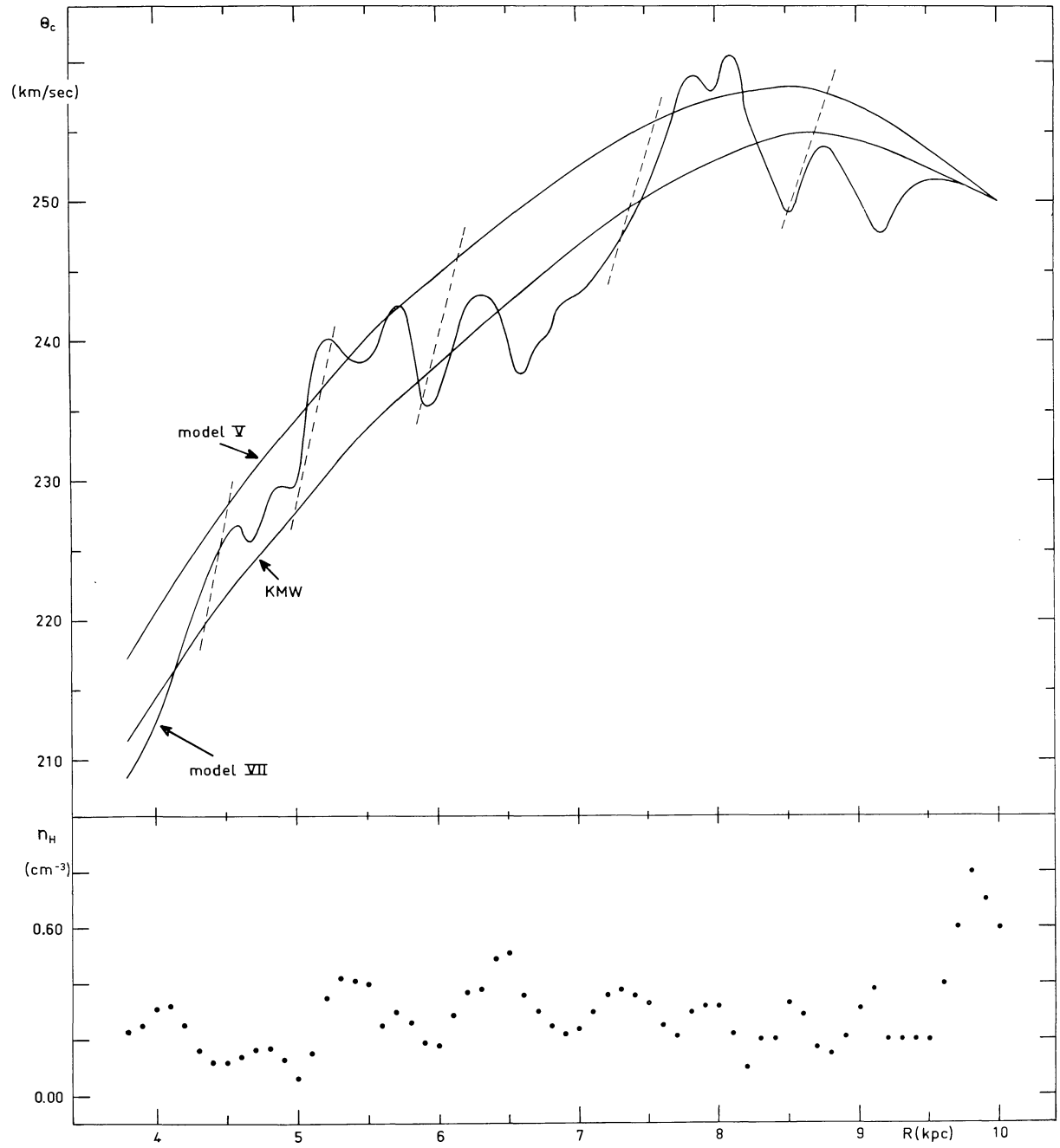

Figure 12. Parameters derived from model VII. The upper diagram shows the model VII rotation curve along with that used for model V and the original KMW curve. The broken lines show the run of solid-body rotation in several regions. The lower diagram shows the run of H I density adopted for model VII. As explained in the text, the values of n_H shown here are probably not typical of the real neutral hydrogen density in the galactic plane.

maximum ordinates, and a similar procedure is implicit in the determination of V_x from equation (5).

In addition to the hydrogen density $n_H(R)$, both the rotational velocity $\Theta_c(R)$ and the velocity dispersion $\sigma(R)$ were introduced into the model as free parameters. In order to avoid an excessive flexibility in the model, $\sigma(R)$, whose adopted values will not influence strongly the derived values of $\Theta_c(R)$, was represented by equa-

tion (6). This representation, in qualitative agreement with the discussion of SCHMIDT (1957), seems to reproduce the observed steepness of the line profiles reasonably well.

The other two parameters were adjusted by trial and error, beginning with a uniform hydrogen distribution and the KMW rotation curve. The final values are listed in columns 4 and 5 of table 5 and are plotted in figure 12. The upper part of the figure shows the rotation curve $\Theta_c(R)$ along with the KMW curve, which is seen to represent an excellent mean of the model VII curve, and the smooth rotation curve adopted for model V. The broken lines represent solid-body rotation. The lower part of figure 12 shows the adopted density variation, $n_H(R)$. It should be noted that this is not a very satisfactory representation of the real hydrogen density. The variation was introduced for the purpose of matching the heights of the observed and computed line profiles near their terminations. Just at these points the heights will depend critically upon the detailed behaviour of the velocities in the vicinity of the tangent points, as this will determine the path lengths over which the hydrogen contributes to the terminal peaks. In this model the behaviour of these velocities is specified by the run of $\Theta_c(R)$ which has been introduced to represent the sequence of line profiles. These values may well be inappropriate for the specification of the run of velocity along a given line of sight near its tangent point, representing failure of our approximation of circular symmetry over small sectors in the tangential region.

The criteria used in matching the computed to the observed line profiles have been discussed in section 3, and the results may be seen in figures 4–6 where the line profiles computed from model VII are plotted as solid curves. The striking tendency for the computed curves to fall below the observations at lower velocities, which is a result of attempting the best possible match in the highest velocity portions of the line profiles, may represent some particular feature of the hydrogen motions, such as the frequent occurrence of two or more streams with different velocities in the same general region. The highest velocity stream, which would determine the velocity $\Theta_c(R)$ as derived here, would be responsible for the termination of the line profile, while other streams would appear as lower velocity maxima. The possible existence of such effects is suggested by more extensive surveys in the region studied here (BURTON, 1966). In any case, the observed systematic discrepancy emphasizes the weakness of the determination of $n_H(R)$ and suggests that the surprisingly low values derived may be accounted for by supposing that only a part of the neutral hydrogen present near the tangent point contributes to the highest velocity portion of the line profile.

The predicted line profiles plotted in figures 4–6 were computed from the final model with the aid of the Electrologica X1 computer of the Leiden University. The main computing program was written in Algol 60 language. The method of computation was as follows.

1) A line profile in optical depth was introduced, $\tau(V)$, where V was assigned integral values in km/sec over the velocity range of interest. All $\tau(V)$ were given initial values of zero.

2) The line of sight was divided into intervals of 100 pc beginning at the tangent point. The path length corresponding to each interval was 200 pc because of the symmetry about the tangent point.

3) At the centre of each interval the hydrogen density, the velocity with respect to the local standard of rest and the velocity dispersion were determined from the model.

4) The contribution from each interval was added to each point on the line profile within the range $\pm 3\sigma$ of the central velocity. The contribution of a 200 pc line segment at a mean distance R from the galactic centre to the optical depth at velocity V_0 is

$$\Delta\tau(V_0) = \frac{134.2\, n_H(R)}{\sigma(R) T_g} \exp\left\{ -\tfrac{1}{2} \left[\frac{V - V_0}{\sigma(R)} \right]^2 \right\}, \qquad (36)$$

where V is calculated from equation (17). Successive intervals along the line of sight were considered until no more significant contributions were made in the part of the line profile to be calculated.

5) The line profile, expressed in terms of optical depth, was converted to brightness temperature by the inverse of equation (1), with an assumed gas temperature $T_g = 130$ °K.

6) The terminal velocity V_x was determined for the calculated line profiles from equation (5). The values of V_x from equation (5) were not used in adjusting the model, as the direct comparison of line profiles was considered preferable, but they are listed in column 7

of table 1, where they may be compared with the observed values listed in column 5. The agreement is quite poor for many profiles, but this may be attributed to the fact that the values of V_x computed from the model profiles are based on values of V_M determined by the computing program as the first maxima in the line profiles. As these first maxima were frequently quite far from the ends of the profiles, the values of V_M differed seriously from those used in analyzing the observed profiles. The strong dependence of this method upon the shape of the line profile in the region of the peak, which is of secondary importance in determining the rotation curve, has dictated our use of direct comparison.

An examination of figure 12, along with reference to figures 4–6, enables us to interpret the results of the model VII calculations in terms of the neutral hydrogen distribution and kinematics in the neighbourhood of the locus of tangent points. We emphasize again that the method applied here yields information about only a very restricted region of the Galaxy along this locus. But whereas nothing can be said about the behaviour of the neutral hydrogen in other regions, there is no reason to believe that the region studied here is atypical of the Galaxy as a whole, although the existence of large-scale asymmetries has been indicated. As shown in section 4 the presence of radial motions of the hydrogen will not lead to very serious consequences with regard to the interpretation of the observed velocities. The most important effect of such motions will be to shift the position of the velocity maximum away from the tangent point. Radial motion of the local standard of rest, on the other hand, will affect the observed velocities in an important but easily calculable way.

The most prominent features of the model VII rotation curve are the maxima at $R = 5.5$ and 8.0 kpc. These correspond to the maxima found by KMW and to the intersection of the locus of tangent points with the arms in their model, the Kootwijk map and our model V. The absence of a maximum in the model VII density distribution at the second of these points emphasizes that maxima in the rotation curve of the sort observed here can be sufficient in themselves to cause the appearance of density maxima near the corresponding tangent points when the interpretation is based upon the KMW or the model V assumptions. This is not to say that the two arms seen in the Kootwijk map and in model V are not real. The maxima in the rotation curve may well be the dynamical results of density fluctuations, as suggested by SCHMIDT (1956), in which case the density maxima will lie somewhat inward from the velocity maxima. Nevertheless, if model VII rather than model V represents the more valid interpretation of the observations, the results of model V and the Kootwijk survey must be considered in the light of the above remark.

While the model VII density distribution shows no maximum in the neighbourhood of the Sagittarius arm, as defined by the rotation curve, a maximum does occur in the neighbourhood of the inner arm, about $R = 5.4$ kpc. It is striking that in the inner region of the Galaxy, $R < 7$ kpc, the density variation follows roughly the run of the rotation curve. For $R > 7$ kpc, on the other hand, the trend seems to be reversed, minima in the density distribution corresponding with maxima in the rotation curve. This seems to indicate that there is some essential structural difference between these two regions. Possibly a large fraction of the hydrogen in some of the regions of greatest density is in molecular form. The suggestion that the peak just short of the maximum velocity in the line profiles at $l = 50°$ to 55° is the density maximum associated with the Sagittarius arm (BURTON, 1966) explains the absence of a maximum in $n_H(R)$ in this region.

At several places in figure 12, broken lines indicate the run of solid-body rotation. In only one region, around $R = 5.0$ kpc, does the slope of the $\Theta_c(R)$ curve exceed the solid-body relation. At this point the assumption that the highest velocity will be encountered at the tangent point fails. The rapid changes in form of the observed line profiles made adjustment of the model very difficult in this region. In particular, the sudden increase in terminal velocity observed between $l = 29°.3$ and $l = 30°.3$ could not be reproduced by any set of values of the parameters. The steep slope of the $\Theta_c(R)$ curve above the point at $R = 5.0$ kpc was introduced in an effort to represent these profiles. The effect is that the termination at $l = 29°.3$ is defined by the hydrogen in the velocity maximum at $R = 5.2$ kpc. The values of Θ_c and n_H assigned at $R = 5.0$ kpc are no longer important in defining the model line profiles. In particular, the low value of $n_H(5.0)$ is without significance. Consequently, a further steepening of the $\Theta_c(R)$ relation in this region could not improve the fit. Although

the slope of $\Theta_c(R)$ approaches the solid-body value in some other regions, the case discussed above was the only one in which the fit remained unsatisfactory.

The maximum in $\Theta_c(R)$ at $R = 5.5$ kpc is broad and complex. The rotation curve adopted for model V passes through both peaks, which thus give slightly forbidden velocities on the basis of that model. The dip between these two peaks might be represented as a gap between two branches of the arm, but this detail has been omitted from figure 10. Turning to the representation by model VII, we see from figure 4 that the match between computed and observed line profiles is considerably better here than at the lower longitudes. Even the maximum heights are reasonably well represented, except at $l = 34°.3$. The unusual line profile at $l = 35°.3$ is quite well represented by the model, although it was not generally within the scope of the model to reproduce this sort of detail.

The prominent maximum in the rotation curve at $R = 6.3$ seems to coincide with the occurrence of a strong maximum in the line profiles just shortward of the termination. The subsequent drop in velocity may result in part from the appearance of this maximum at the terminations of the line profiles around $l = 41°$. One of the highest maxima in the density distribution corresponds with this drop in rotational velocity.

Over the next few degrees the model represents the observations well and the rotation curve shows little detail. At $l = 50°$, however, a strong feature makes its appearance somewhat shortward of the maximum velocity. This feature increases in strength and approaches the termination of the line profiles until it reaches a maximum at about $l = 55°$. Thereafter it disappears rapidly, without ever having reached a sufficiently high velocity to influence $\Theta_c(R)$ or $n_H(R)$. This is the feature that has been mentioned above as possibly associated with the density maximum in the Sagittarius arm.

The maximum in the rotation curve at $R = 8.0$ kpc is narrow and well-defined. The velocities here are slightly forbidden with respect to the rotation curve adopted for model V, while the narrowness of arm C reflects the sharpness of the peak. The drop in $\Theta_c(R)$ for $R > 8.1$ kpc is well defined as is the secondary maximum at $R = 8.8$ kpc. Except for the remarkable projection at $l = 63°$, the observations are reasonably well represented for the remaining longitudes through $l = 66°$. At $l = 67°$ and $68°$ the forms of the line profiles deviate strongly from anything that can be reproduced by the model, but the computed profiles seem to provide as good a match as can be hoped for. For the last two profiles the match is again satisfactory.

The highest longitude observed, $l = 70°$, corresponds to a tangent point at $R = 9.4$ kpc. The trend of $\Theta_c(R)$ and $n_H(R)$ for higher values of R, up to $R = 10$ kpc, was determined by the matching requirement for the last profiles and by the requirement that $\Theta_c(10) = 250$ km/sec. It was convenient to let the adopted rotation curve coincide with the KMW curve in the immediate neighbourhood of $R = 10$ kpc.

The failure of model VII to produce profiles which more closely match the observations is due largely to our assumption of circular symmetry. Abandoning this assumption, however, would lead to such a multitude of possibilities that no unique determination of the rotation curve would be possible. In addition to the assumption of circular symmetry, we have found it desirable to neglect irregularities in the run of $\sigma(R)$, which are certainly present. Even with these restrictions there might be some doubt as to the uniqueness of our determination. We feel, however, that once we have determined which part of each observed profile is to be represented by the model, the required values of $\Theta_c(R)$ and $n_H(R)$ will be uniquely determined in most cases. With the exception of $l = 67°$ and $68°$, we have tried to adjust n_H in such a way that the height of the computed profile corresponds with the height of the observed profile up to the first prominent break or shoulder. This procedure has been justified above and was required by the restrictions of the model, which made it impossible, except under certain fortuitous circumstances, to represent more than a single smooth descending branch at each longitude.

5. Summary and conclusions

In the above analysis we have interpreted our observations on the basis of two alternative models. In constructing model V, we have assumed that the rotation curve is a smooth function of galactocentric distance and that the shape of each line profile is determined entirely by the distribution of neutral hydrogen along the line of sight. Such a model is capable of representing any conceivable set of line profiles, provided the rotation curve is drawn high enough; the validity of the model can be judged only on the basis of the plau-

sibility of the resulting density distribution. We found, in this case, from examination of the model VI results, that model V could explain the observations only if a very low hydrogen density were assumed in the inter-arm region, averaging 1 per cent or less of the density in the arms. Although it is difficult to reject the model altogether on this ground, it yields a picture so in conflict with our impression of other galaxies that we are inclined to prefer model VII. This model assumes the presence of a substantial amount of hydrogen in all regions of the galactic plane, so that the maximum velocity seen in each direction is that of hydrogen near the tangent point. Under these circumstances, the assumption of circular symmetry made in model VII becomes more acceptable than it was, for example, in model IV. From such a model we can derive a rotation curve which is largely independent of the details of the assumed hydrogen distribution. We have compared the results of this model with the observations in some detail and have seen that the model is capable of representing only a very small part of each line profile. The limited ability to represent the observations emphasizes the shortcomings of model VII. Some possible explanations of the failures of model VII have been suggested in the course of the discussion. It appears that large-scale streaming motions with velocities in the neighbourhood of 10 km/sec and breadths of several tens to several hundreds of parsecs may play an important part in the general picture of galactic hydrogen motion.

Although models V and VII are mutually exclusive, the first requiring a smooth rotation curve and the second yielding an irregular one, an attractive compromise is available. We can consider a galaxy of the form suggested by model V in which the neutral hydrogen in the unshaded region in figure 10 is not of particularly low density but rather is moving about the galactic centre with a velocity substantially lower than that which defines the maximum velocity. It need not be true that the density maxima and the velocity maxima coincide, provided only that there be sufficient hydrogen located as shown schematically in figure 10 and moving with the velocities given by the model V curve in figure 12. The hydrogen in the vicinity of those tangent points which do not lie within the streams must be moving with velocities no greater than those given by the model VII curve. The apparent rotation curve as represented by model VII may, indeed, be defined at some points by the fast moving streams and at others, particularly near its minima, by slower moving hydrogen. This would permit us to draw more circular arms than those shown in figure 10 without requiring an increase in the depth of the minima of the apparent rotation curve.

Unfortunately the data at our disposal are insufficient to test this hypothesis adequately. In the course of an extensive study of the region in which the Sagittarius arm is seen tangentially, BURTON (1966) has found evidence that the densest part of the arm is bounded on its outer edge by a stream of hydrogen which appears to have a singularly high velocity in the direction of galactic rotation. The observations discussed here are entirely compatible with this interpretation, and a similar phenomenon may be responsible for the observed maximum in the rotation curve at $R = 5.5$ kpc, although the structure in the inner region appears to be more complex.

Figure 12 shows that none of the model rotation curves discussed here falls substantially below the KMW curve, thus confirming the large-scale asymmetry with respect to the galactic centre. If the highest observed velocities are due primarily to streams such as those discussed above, then the behaviour of these streams will be important in determining the nature of the asymmetry.

We conclude that the rotation curve derived from model VII is the best estimate that we can make from these observations of the galactic rotation curve as sampled along the semi-circle of tangent points. The details shown are certainly local features not present over large ranges of galactocentric longitude. The major features are probably associated with the spiral arms. The maxima are most probably accurate measures of the velocities at the corresponding tangent points. Other parts of the curve may also represent velocities at the corresponding tangent points or they may be defined by high-velocity hydrogen located elsewhere along the line of sight. In the latter case, we expect this high-velocity hydrogen to be located approximately as shown in figure 10. The model VII curve in figure 12 will then be an upper limit to the rotation curve appropriate to the lower-velocity hydrogen. A state of affairs in which part of the measured curve is defined in the one way and part in the other is quite plausible.

Acknowledgements

We are greatly indebted to Professor J. H. Oort for many valuable suggestions and to Dr. F. J. Kerr for permitting us to use his results in figure 1 and for his helpful interest. This work was supported in part by the Netherlands Organization for the Advancement of Pure Research (Z.W.O.).

References

T. A. Agekyan, I. V. Petrovskaya and B. I. Fessenko, 1964, *Astr. Zhur.* **41** 1027
L. L. E. Braes, 1963, *Bull. Astr. Inst. Netherlands* **17** 132
W. B. Burton, 1966, *Bull. Astr. Inst. Netherlands* **18** 247
M. W. Feast, 1964, *Symp. I.A.U.-U.R.S.I.* No. 20 67
M. W. Feast and M. Shuttleworth, 1965, *Mon. Not. Roy. Astr. Soc.* **130** 245
J. Högbom and L. Volders, 1961, *Bull. Astr. Inst. Netherlands* **15** 307
I.A.U., 1964, *Trans. I.A.U.* **12A** 523
N. S. Kardashev, T. A. Lozinskaya and N. F. Sleptsova, 1964, *Astr. Zhur.* **41** 601
F. J. Kerr, J. V. Hindman and C. S. Gum, 1959, *Australian J. Phys.* **12** 270
F. J. Kerr, 1962, *Mon. Not. Roy. Astr. Soc.* **123** 327
F. J. Kerr, 1964, *Symp. I.A.U.-U.R.S.I.* No. 20 81
F. J. Kerr, 1965, *Australian J. Phys.*, in press
K. K. Kwee, C. A. Muller and G. Westerhout, 1954, *Bull. Astr. Inst. Netherlands* **12** 211
G. Münch and L. Münch, 1960, *Ap. J.* **131** 253
E. Raimond, 1966, *Bull. Astr. Inst. Netherlands Suppl.* **1** 33
M. Schmidt, 1956, *Bull. Astr. Inst. Netherlands* **13** 15
M. Schmidt, 1957, *Bull. Astr. Inst. Netherlands* **13** 247
W. W. Shane, 1966, *Bull. Astr. Inst. Netherlands*, in preparation
G. Westerhout, 1957, *Bull. Astr. Inst. Netherlands* **13** 201
H. van Woerden, G. W. Rougoor and J. H. Oort, 1957, *Comptes Rendus Acad. Sci. Paris* **244** 1691
H. van Woerden, K. Takakubo and L. L. E. Braes, 1962, *Bull. Astr. Inst. Netherlands* **16** 321